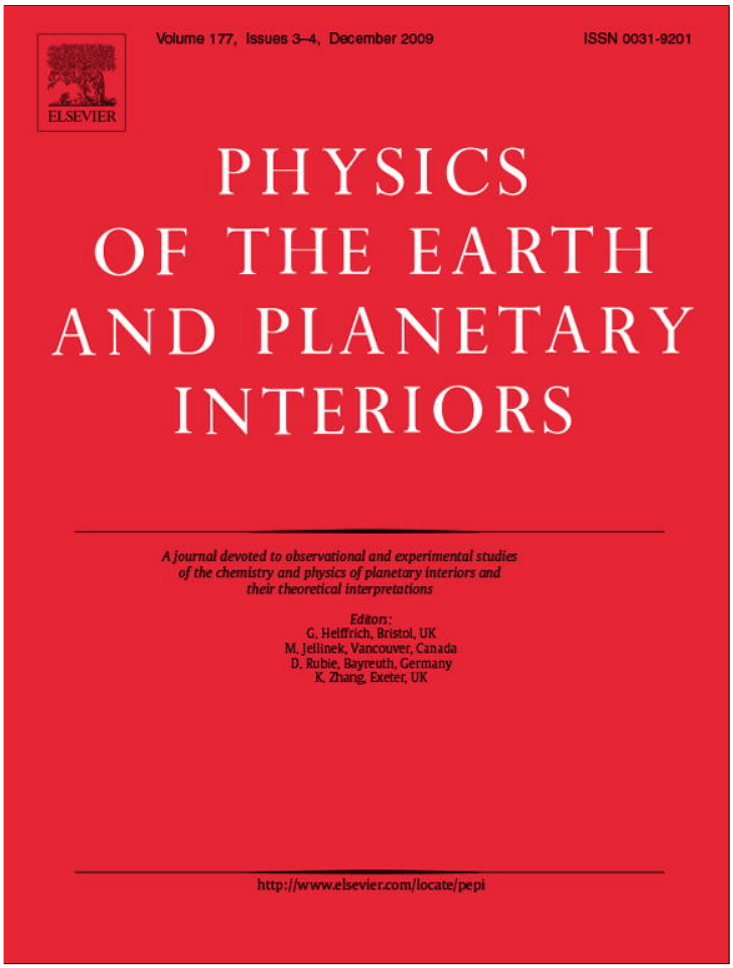

Physics of the Earth and Planetary Interiors 177 (2009) 217–234

Contents lists available at ScienceDirect

Physics of the Earth and Planetary Interiors

journal homepage: www.elsevier.com/locate/pepi

3D density model of the Central Andes

Claudia B. Prezzi [a,*], Hans-Jürgen Götze [b], Sabine Schmidt [b]

[a] CONICET, Universidad de Buenos Aires. INGEODAV, Dpto. de Cs. Geológicas, FCEyN, Universidad de Buenos Aires. Ciudad Universitaria, Pabellón 2, 1428, Buenos Aires, Argentina
[b] Institut für Geowissenschaften, Abteilung Geophysik, Christian Albrechts Universität, Otto-Hahn-Platz 1, 24118 Kiel, Germany

ARTICLE INFO

Article history:
Received 21 January 2009
Received in revised form 7 September 2009
Accepted 22 September 2009

Edited by: M. Jellinek.

Keywords:
Central Andes
Gravity
3D density model
Lithospheric structure

ABSTRACT

We developed a 3D density model of the continental crust, the subducted plate and the upper mantle of the Central Andes between 20–29°S and 74–61°W through the forward modelling of Bouguer anomaly. The goal of this contribution is to gain insight on the lithospheric structure integrating the available information (geophysical, geologic, petrologic, and geochemical) in a single model. The geometry of our model is defined and constrained by hypocentre location, reflection and refraction on and offshore seismic lines, travel time and attenuation tomography, receiver function analysis, magnetotelluric studies, thermal models and balanced structural cross-sections. The densities allocated to the different bodies are calculated considering petrologic and geochemical data and pressure and temperature conditions. The model consists of 31 parallel E–W vertical planes, where the continental crust comprises distinct bodies, which represent the different morphotectonic units of the Central Andes. We include a partial melting zone at midcrustal depths under the Altiplano-Puna (low-velocity zone) and consider the presence of a rheologically strong block beneath the Salar de Atacama basin, according to recent seismic studies. Contour maps of the depth of the continental Moho, the thickness of the lower crust and the depth to the bottom of the lithosphere below South America are produced. The possible percentage of partial melt in the Central Andes low-velocity zone is estimated. The residual anomaly is calculated by subtracting from the Bouguer anomaly the gravimetric effect of the modelled subducted slab and of the modelled Moho. Isostatic anomalies are calculated from regional and local isostatic Mohos calculated with and without internal loads, derived from our gravity model, which are then compared to the modelled continental Moho. This study contributes to a more detailed knowledge of the lithospheric structure of this region of the Andes and provides an integrated 3D density model, which may be used by the geoscientific community as a tool that can help to understand and interpret the geodynamic features and processes acting along the Central Andes.

1. Introduction

The Central Andes present outstanding and unique features challenging any geoscientific research. One of these is the Altiplano-Puna plateau. It is approximately 2000 km long, 300 km wide and 3700 m in average elevation and dominates the physiography of the Central Andes. The Altiplano-Puna is the highest plateau in the world associated with abundant arc magmatism, and is second only to Tibet in height and extent. It was uplifted in the absence of continental collision or terrane accretion (Allmendinger et al., 1997; Lamb, 2000). Its uplift is related to the subduction of the ~40 Ma old oceanic Nazca plate (Müller et al., 1997) beneath the continental South American plate (Jordan et al., 1983; Isacks, 1988; Allmendinger et al., 1997). Recent seismic experiments (Yuan et al., 2000; Yuan et al., 2002; ANCORP, 2003) determined crustal thickness under the Altiplano-Puna of approximately 70 km, suggesting that thickening is associated with compressional shortening of a weak lithosphere squeezed between the subducting Nazca plate and the Brazilian shield.

Interdisciplinary research was carried out by geoscientists of the Collaborative Research Centre SFB 267 "Deformation Processes in the Andes". Along a W–E segment between the latitude of 20°S and 26°S, this project aimed to achieve more insight into the lithospheric structure and to decipher recent and past processes forming this orogenic belt. This interdisciplinary approach applied a variety of geophysical, geodetic, geologic and petrologic methods, producing a wealth of geophysical and geologic information and probably making the Central Andes the geophysically most densely covered convergent continental margin. We developed a 3D model of the density structure of the Central Andes (between 20–29°S and 74–61°W) through a 3D forward modelling of the Bouguer anomaly. Kirchner et al. (1996) published a 3D density model for the Central Andes, where the constraining data were virtually lim-

* Corresponding author. Tel.: +54 11 4788 3439; fax: +54 11 4788 3439.
E-mail addresses: prezzi@gl.fcen.uba.ar (C.B. Prezzi), hajo@geophysik.uni-kiel.de (H.-J. Götze), sabine@geophysik.uni-kiel.de (S. Schmidt).

0031-9201/$ – see front matter © 2009 Elsevier B.V. All rights reserved.
doi:10.1016/j.pepi.2009.09.004

ited to wide-angle seismic refraction experiments. Therefore, their model was almost entirely based and resembled the results of refraction seismics, with the velocities of the seismic models being directly converted into densities. Recently, a 3D density model of the Andes between northern Perú (5°S) and Patagonia (45°S) was presented by Tassara et al. (2006). Their model is composed of a minimum number of bodies and is a continental-scale representation of the density structure. Tassara et al. (2006) noted that their model can be used to analyze first-order variations at the scale of the entire Andean margin, but it does not consider the details of regional and local structures. On the other hand, our regional-scale gravity model shows a higher degree of detail, summarizing and integrating all the above-mentioned information. Therefore, the detailed 3D density structure obtained for the Central Andes is constrained by a huge amount of data published in the last years (e.g. Lucassen et al., 2001; Yuan et al., 2002; Brasse et al., 2002; ANCORP, 2003; Schurr and Rietbrock, 2004; Heit et al., 2008). The major goals of this work are to contribute to a more detailed knowledge of the lithospheric structure of this region of the Andes and to provide an integrated 3D density model, which may be used by the geoscientific community as a tool that can help to understand and interpret the geodynamic features and processes acting along the Central Andes.

2. Geologic setting

From W to E, the Central Andes can be divided into forearc, magmatic arc and backarc (Fig. 1). The forearc comprises the Coastal Cordillera, the Longitudinal Valley, the Chilean Precordillera and the Preandean depression. The magmatic arc is represented by the Western Cordillera. The backarc consists of different morphotectonic units: the Altiplano-Puna, the Eastern Cordillera, the Subandean Ranges, the Santa Bárbara System and the Chaco foreland.

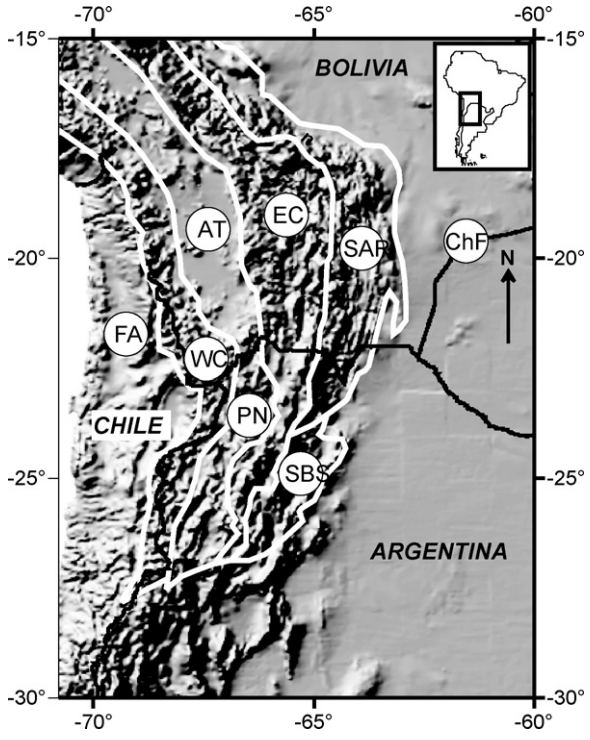

Fig. 1. Shaded relief topography (GTOPO30 digital elevation model) showing the different morphotectonic units identified in the Central Andes. Inset shows the study area with relation to South America. FA: Forearc, WC: Western Cordillera, AT: Altiplano, PN: Puna, EC: Eastern Cordillera, SAR: Subandean Ranges, SBS: Santa Bárbara System, ChF: Chaco Foreland.

The Coastal Cordillera is principally built up by Jurassic to Lower Cretaceous basic to andesitic volcanic and plutonic rocks. The Chilean Precordillera consists of Paleozoic basement, Mesozoic and Tertiary sedimentary and volcanic rocks, and it is intruded by Late Cretaceous to Paleogene plutons (Scheuber et al., 1994). The present day magmatic arc is represented by the Western Cordillera. Note that the magmatic arc of the Central Andes has been displaced (~200 km) since Early Jurassic from the Coastal Cordillera to the Western Cordillera with four successive arc systems (Coira et al., 1982; Scheuber et al., 1994). The Altiplano-Puna plateau is a wide intramountainous basin with Mesozoic–Cenozoic sedimentary infill reaching thicknesses of up to 10 km. The plateau overlies a 30° east-dipping segment of the Nazca plate; north of 12°S and south of 28°S the slab is dipping gently and an internally drained plateau is absent (Jordan et al., 1983; Isacks, 1988). In the region of steep dip, basaltic–andesitic volcanism is active, while recent volcanic activity is not detected to the north and south. Local volcanic edifices are present within the plateau. The volcanic arc and local volcanic centres have been active from Miocene to present time (Jordan and Gardeweg, 1989; Schurr and Rietbrock, 2004). Since the late Miocene, an ignimbrite "flare-up" produced a major volcanic province, the Altiplano-Puna Volcanic Complex (APVC) (de Silva, 1989; Zandt et al., 2003). The APVC covers approximately 50,000 km^2 between 21°S and 24°S. Partial melt was proposed by Heinsohn (1993) beneath broad parts of the Altiplano plateau based on gravimetric modelling. Chmielowski et al. (1999) identified a very low-velocity layer at a depth of 19 km, which they interpreted as a regional sill-like magma body associated with the APVC. Yuan et al. (2000) detected an intracrustal low-velocity zone below the entire Altiplano-Puna. They interpreted it as a zone of continuing metamorphism and partial melting that decouples upper-crustal imbrication from lower-crustal thickening. Implications of the partial melting were discussed by Schilling et al. (1997, 2006). The Altiplano-Puna is bounded by the Western Cordillera to the west and by the tectonic highlands of the Eastern Cordillera to the east (Fig. 1). The Eastern Cordillera is mainly composed of Precambrian to Paleozoic rocks, covered by Cretaceous and Cenozoic sediments. Since the Miocene, ongoing contractional deformation generated a fold-thrust belt system in the backarc region of the Central Andes, now represented by the Subandean Ranges and the Santa Bárbara System (Fig. 1). While the Subandean Ranges are a thin-skinned fold and thrust belt, the Santa Bárbara System is a thick-skinned thrust belt (Kley et al., 1999). Up to 7.5 km of Cenozoic sediments have been deposited since the late Oligocene in the Chaco foreland basin.

3. The model

3.1. Gravity data base

Offshore Bouguer anomalies were calculated from the 2001 KMS global free-air anomaly data base (Andersen and Knudsen, 1998) considering GEBCO bathymetry (www.ngdc.noaa.gov/mgg/gebco/gebco.html) and replacing ocean water with material of density 2.67 Mg/m^3. Onshore gravity data correspond to measurements made and compiled under the umbrella of the German Collaborative Research Centre SBF 267 "Deformation Processes in the Andes" (for a detailed explanation of compilation, field work and gravity reductions see Götze et al., 1990 and Götze and Kirchner, 1997). We considered 6500 gravity measurements covering an area extending between 20–29°S and 74–61°W (Fig. 2).

Positive values characterize the offshore Bouguer anomaly, with the Perú–Chile trench depicted by strong gradients (Fig. 2). Onshore, the Bouguer anomaly drops down to a minimum of about -450×10^{-05} m/s^2 below the Western Cordillera. Negative values

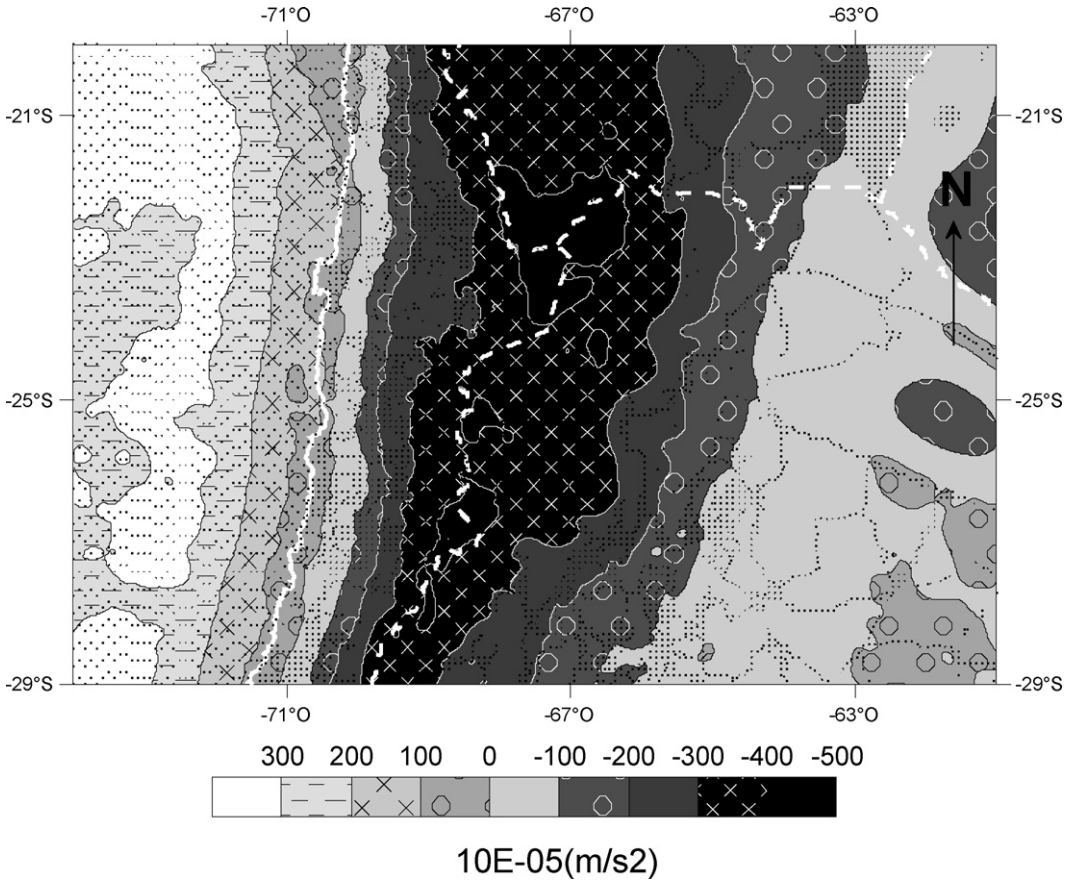

Fig. 2. Bouguer anomaly map of the studied region with contours every 100×10^{-05} m/s^2. White line: coast line. Dashed white lines: political borders. Dots: location of gravity stations.

correlate with the high topography of the orogen. Positive anomalies are observed in the foreland and along the Coastal Cordillera.

3.2. 3D forward modelling software

The interactive forward modelling software IGMAS is used. The acronym stands for "Interactive Gravity and Magnetic Application System" and essentially uses triangulated polyhedrons to approximate areas of constant density and/or susceptibility within the Earth's crust and mantle. The numerical algorithms were developed by Götze (1984) and permit the calculation of geoid, gravity field and its gradients as well as magnetic field components and components of remnant and induced magnetic fields in one program step. The software package IGMAS eases the 3D interpretation of gravity and magnetic data bases. It uses an interoperable 3D Geoinformation System (IOGIS) and its functions (e.g. data queries, interoperability, visualization and interdisciplinary interpretations in an object-oriented data environment) to integrate other geophysical models, information, and data from both geophysics and geology (Breunig et al., 2000; Schmidt and Götze, 1999, http://www.gravity.uni-kiel.de/igmas). The initial geometries of the 3D modelled bodies are predefined by the user on a series of parallel vertical cross-sections. The automated triangulation of model surfaces between the parallel vertical cross-sections, allows the construction of even complicated model geometries. In this work, density values for the modelled bodies are defined prior to the gravity modelling (see Section 3.6). The optimal fit between observed and calculated anomalies is achieved during forward modelling by iterative geometry changes introduced by the user, according to the constraining information incorporated in the IOGIS. That is to say, the user manually modifies the geometry of the different bodies composing the 3D density model, in view of the additional geological and geophysical information integrated in the model. The final model should minimize the differences between observed and calculated Bouguer anomalies (i.e. residual anomalies). Residual anomalies should have lower amplitude than the estimated error in the observed Bouguer anomaly (~±30 mGal), and should show a tight concentration around zero with low standard deviation. The modelled anomaly is calculated from the contrast between the density values assigned to the modelled bodies and the densities of a background reference model.

3.3. Background reference density model

The gravity measured in each station is influenced by the mass of the whole earth, but usually only a small part of the earth is considered in most models. This situation causes an offset between measured and modelled signals. Such offset can be eliminated by introducing a reference model in the background of the density model (e.g. Kirchner et al., 1996). In this work we use a reference model comprising three horizontal layers, which represent the structure and densities of continental crust and upper mantle. The first layer is 15 km thick and depicts the upper crust with a density of 2.67 Mg/m^3. The second layer corresponds to the lower crust, has a thickness of 20 km and a density of 2.90 Mg/m^3. The third layer extends to 220 km depth, representing the upper mantle with a density of 3.35 Mg/m^3. This selected reference model is in good accordance with the worldwide compilation of Christensen and Mooney (1995) and with the work of Rudnick and Fountain (1995), and it is similar to the reference model used by Tassara et al. (2006) in his continental-scale 3D density model of the Andes.

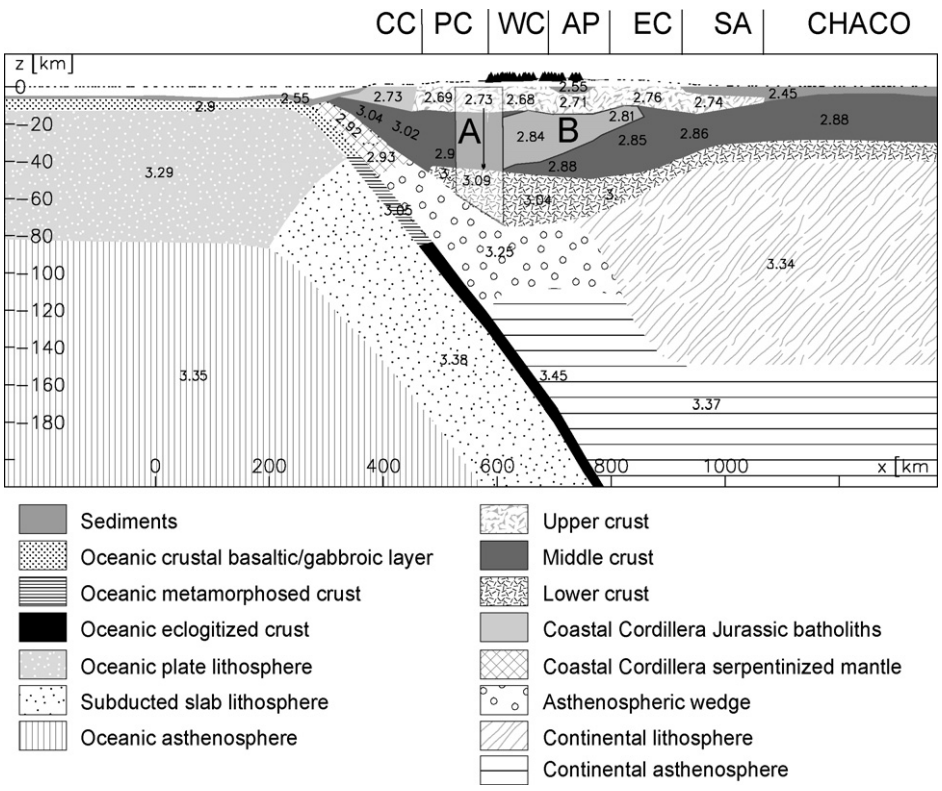

Fig. 3. One of the vertical planes composing the 3D model (located at 22°17′S), showing the initial density structure proposed (i.e. before forward modelling) (density values in Mg/m^3). CC: Coastal Cordillera, PC: Chilean Precordillera, WC: Western Cordillera, AP: Altiplano-Puna, EC: Eastern Cordillera, SA: Subandean Ranges, A: Atacama block, B: Altiplano-Puna partial melting zone. Triangles: position of active volcanoes.

3.4. Model structure

Our model consists of 31 parallel E–W planes extending between 12–35°S and 57–79°W. The density model proposed here extends down to 220 km depth and is characterized by an E–W division of the continental crust into distinct bodies, which strike N–S and correspond to the major morphotectonic units of the Central Andes: Coastal Cordillera, Chilean Precordillera, Western Cordillera, Altiplano-Puna, Eastern Cordillera, Subandean Ranges/Santa Bárbara System and Chaco (Fig. 3). Such bodies are composed by sub-units which correspond to the upper, mid and lower continental crust. The oceanic crust is modelled taking into account the presence of a ~2 km thick sedimentary layer and a ~6 km thick basaltic/gabbroic layer. The eclogitization of the slab

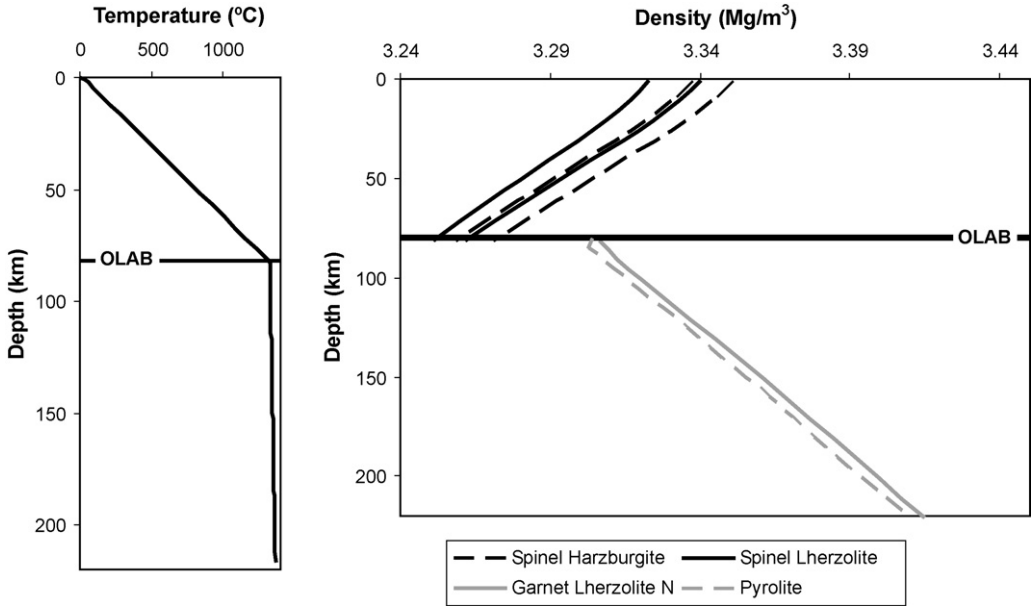

Fig. 4. Left: temperature gradient computed for the oceanic plate, from which a depth of approximately 80 km can be inferred for the oceanic lithosphere–asthenosphere boundary (OLAB). Right: density profiles calculated along such thermal gradient for spinel harzburgites and lherzolites, garnet lherzolite N and pyrolite of Hacker and Abers (2004). The depth of the oceanic lithosphere–asthenosphere boundary (OLAB) is also shown.

during subduction at depths between 60 km and 80 km is contemplated in the model through an increment in its density. The model also includes the continental and oceanic lithosphere, the continental and oceanic asthenosphere, and the asthenospheric wedge.

We include a partial melting zone at midcrustal depths under the Altiplano-Puna, which coincides with the Andean low-velocity zone confined by the intracrustal converters TRAC1 and TRAC2 identified by Yuan et al. (2000). We also consider the presence of a rheologically strong block beneath the Salar de Atacama basin, according to recent seismic studies (Fig. 3). Schurr and Rietbrock (2004) found that crust and mantle beneath the Salar de Atacama basin differ strongly in their seismic properties (high Q_p and v_p) from their surroundings.

3.5. Constraints of model geometry

3.5.1. Oceanic plate

The geometry of our model is constrained by a wealth of geophysical and geologic data. The top and the Moho of the subducting slab have been imaged by seismic reflection and refraction profiles and receiver function analysis. We have digitized and included in the model the depths to these discontinuities documented by the following authors. Patzwahl et al. (1999) interpreted seismic refraction/wide-angle reflection data from CINCA95 project and produced nine E–W 2D velocity cross-sections for the region between the Perú-Chile trench and the coast between 19.5°S and 25°S, with three of the cross-sections extending 100–200 km farther inland. Bock et al. (2000) obtained a high-resolution image of the oceanic Moho in the subducting Nazca plate at 24°S from *P–S* converted waves. Yoon et al. (2003) presented the results of prestack depth migration of the PRECORP and ANCORP data sets. PRECORP is a 50 km long seismic reflection line located at 22.5°S, and ANCORP is a combined seismic reflection and refraction experiment with a total length of ca. 385 km, acquired at 21°S (ANCORP, 2003). These images clearly show the upper and lower boundaries of the oceanic crust. Receiver function analysis also imaged locally the slab Moho. Yuan et al. (2000) presented four E–W depth profiles at 19.5°S, 22.5°S, 23.5°S and 24.5°S showing the subducting oceanic Moho. Heit et al. (2008) produced receiver functions results along an E–W profile at 21°S, where the top of the slab was clearly observed. In addition, we also use hypocentre locations recorded by local seismic networks (Belmonte, 2002) and seismicity registered at teleseismic distance (Engdahl et al., 1998; USGS NEIC catalogue: http://neic.usgs.gov/neis/epic/epic.html; Centennial Global Earthquake Database: http://www.geonavi.com/eric/HotNews/eqDB.html) compiled by Tassara et al. (2006) to define the geometry of the slab top.

Table 1
Densities assigned to each modelled body and tolerable density variations (in percentage and in Mg/m^3).

	Density (Mg/m3)	Tolerable variation (%)	Tolerable variation (Mg/m3)
Oceanic area			
Oceanic plate			
Ocean water	2.67	2.43	0.065
Crustal sedimentary layer	2.55	5.22	0.133
Crustal basaltic/gabbroic layer	2.9	2	0.058
Lithosphere	3.29	0.24	0.008
Subducted slab			
Metamorphosed cust	3.05	3.84	0.117
Eclogitized crust	3.45	2.9	0.1
Lithosphere	3.38	0.27	0.009
Astenosphere	3.35	0.15	0.005
Continental area			
Upper crust			
Coastal Cordillera	2.73	1.54	0.042
Precordillera	2.69	1.19	0.032
Central Chile	2.65	1.06	0.028
Western Cordillera	2.68	1.08	0.029
Altiplano-Puna sediments	2.55	3.65	0.093
Altiplano-Puna	2.71	1.22	0.033
Eastern Cordillera	2.76	1.34	0.037
Subandean Ranges	2.74	2.04	0.056
Chaco sediments	2.45	2.53	0.062
Middle crust			
Coastal Cordillera	3.02–3.04	1.09–1.82	0.033–0.055
Precordillera	2.9	0.76	0.022
Western Cordillera	2.88	0.83	0.024
Altiplano-Puna	2.88	0.87	0.025
Eastern Cordillera	2.85	0.77	0.022
Subandean Ranges	2.86	1.12	0.032
Brazilian shield	2.88	0.59	0.017
Lower crust			
Coastal Cordillera, serpentinized mantle	2.92–2.93	1.71–2.09	0.05–0.061
Precordillera	3	1.77	0.053
Western Cordillera	3.04	1.35	0.041
Altiplano-Puna	3.04	1.35	0.041
Brazilian shield	3	1.07	0.032
Atacama block	2.74–3.09	0.49–0.55	0.015
Altiplano-Puna partial melting zone	2.81–2.84	0.85	0.024
Lithosphere	3.34	0.15	0.005
Asthenosphere	3.37	0.3	0.01
Asthenospheric wedge	3.25	0.58	0.019

3.5.2. Continental plate

Different authors estimated the depth to the continental Moho. Baumont et al. (2001) carried out an inversion of *Pn* travel times, characterizing the Moho geometry along a profile extending between 19° and 20°S. Beck and Zandt (2002) combined receiver function and surface wave dispersion results to investigate the crustal structure between 17° and 21°S. They calculated the depths to the continental Moho along a profile at 19.5°S. Receiver function analysis between 17° and 25°S has been published by Yuan et al. (2000, 2002). Yuan et al. (2000) presented four E–W depth profiles at 19.5°S, 22.5°S, 23.5°S and 24.5°S showing the continental Moho. Yuan et al. (2002) mapped the Moho topography in greater detail, applying a grid-search algorithm. Heit (2005) and Heit et al. (2008) computed receiver function Moho depths along two profiles at 21° and 25.5°S. Fromm et al. (2004) obtained a 2D crustal model using apparent *Pn* phase velocities recorded along an E–W trending transect at 30°S. The Moho depths reported in all of these works have been digitized and introduced in our model. However, it is worthy to note that differences of up to 15 km exist between the Moho depths calculated for the same locations in the above-mentioned studies. We use average values to define the geometry of our model. We do not use as constraints Moho depths predicted by local or regional isostatic models.

Magnetotelluric data, different tomographic studies, thermal models, seismic lines and structural balanced cross-sections were also digitized and are used to further constrain the geometry of the different crustal bodies, of the asthenospheric wedge and of the continental lithosphere–asthenosphere boundary (CLAB). Schwarz and Krüger (1997) constructed an E–W resistivity cross-section at 21.8°S and detected a high conductivity zone that stretches from the Western Cordillera to the Eastern Cordillera at 25–30 km depth. Brasse et al. (2002) produced a MT model along ANCORP profile at 21°S, and a new 2D inversion result for the PICA profile, which extends between 20.9° and 20°S, was presented by Echternacht et al. (1997). The main geoelectrical structure resolved was a broad and probably deep-reaching highly conductive zone in the middle and deeper crust beneath the plateau. Booker et al. (2004) presented results from a magnetotelluric profile at 31.8°S, from which they inferred enhanced electrical conductivity above the subducting slab. Travel time tomographic images were generated by Graeber and Asch (1999). They published three E–W sections at 22.25°S, 22.75°S and 23.25°S depicting v_p and two E–W sections at 22.75°S and 23.25°S displaying v_p/v_s ratios. Schurr et al. (2003) showed five E–W cross-sections through their 3D model of *P*-wave attenuation (Q_p) at 21.3°, 22.1°, 22.8°, 23.5° and 24.2°S. They identified prominent low Q_p anomalies beneath the magmatic arc and the backarc in the crust and mantle. Another Q_p cross-section at 23.2°S was presented by Schurr and Rietbrock (2004), which revealed high Q_p values beneath the Salar de Atacama basin. A thermal model was developed by Springer (1999) from surface heat-flow density data along a profile at about 21°S from the Perú-Chile trench to the Andean foreland. He proposed a lithospheric thermal structure with a thinned lithosphere beneath the Western Cordillera, Altiplano and western part of the Eastern Cordillera. A line drawing of ANCORP reflection seismic results (ANCORP, 2003) including the Quebrada Blanca Bright Spot (ANCORP, 2003; Yoon et al., 2003) is superposed to the density model. Also the Calama Bright Spot (PRECORP: Yoon et al., 2003) was digitized and is included, in order to investigate any possible correlations between such bright spots and the gravity anomalies. On the basis of refraction seismic data (Wigger et al., 1994; PISCO94: Schmitz et al., 1999), Raytracing v_p models striking N–S and E–W were generated by Lessel (1997) and are incorporated in our model. The nine above-mentioned E–W 2D velocity cross-sections produced by Patzwahl et al. (1999) also provide information about the continental crust. The structure of the uppermost crust is partially known from balanced cross-sections, which extend W–E from the eastern Altiplano-Puna towards the foreland. We introduce in the model the sections prepared by McQuarrie and DeCelles (2001) at 17°S and 20°S, Müller et al. (2002) at 21°S, Schmitz and Kley (1997) at 21.25°S, Allmendinger and Zapata (2000) at 22.25°S, Kley and Monaldi (2002) at 24.2°S and 24.75°S, Cristallini et al. (1997) at 25.5°S, Ramos et al. (2002) at 27°S, 29°S, 31°S and 33°S and Giambiagi and Ramos (2002) at 33.6°S. The crustal structure and the densities proposed for the study area by the global crustal model CRUST 2.0 (http://mahi.ucsd.edu/Gabi/rem.html, Bassin et al., 2000) are also included. A reasonable fit is observed between the densities of CRUST 2.0, which are derived by published velocity/density relations, and the ones calculated in this study (see Section 3.6).

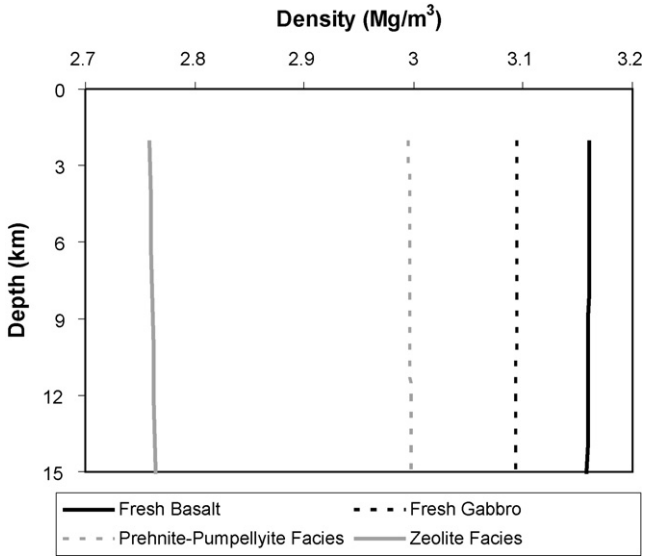

Fig. 5. Density values calculated for an unmetamorphosed MORB and a fresh gabbro, and also for a fully hydrated basalt (zeolite metamorphic facies) and a partially hydrated basalt (prehnite-pumpellyite metamorphic facies) according to the mineralogical compositions proposed by Hacker et al. (2003).

3.6. Calculation of densities

The density values assigned to the different bodies forming the model were calculated on the basis of information and assumptions about the chemical and/or mineralogical composition and pressure–temperature conditions expected for each body (Tassara et al., 2006).

3.6.1. Oceanic plate

To calculate the densities of the oceanic plate we used the Excel Macro of Hacker and Abers (2004), modified by Tassara (2006). The tool designed by Hacker and Abers (2004) calculates density (and other properties) of mafic and ultramafic rocks at a predefined pressure–temperature condition. Tassara (2006) modified the Macro, in order to obtain density vs. depth profiles. In this modified version, the pressure–temperature values are read from a 1D temperature and lithostatic pressure gradient. The temperature gradient is defined by the conductive plate cooling model of Turcotte and Schubert (2002). To compute the temperature gradient we considered an average age for the oceanic lithosphere of 40 Ma (Müller et al., 1997), a thermal diffusivity of 1 mm^2/s (Springer, 1999) and a temperature difference between the top and the bottom of the lithosphere of 1300 °C. The lithostatic pressure gradient was calculated assuming an average density of 3.0 Mg/m^3 and an overpressure factor of 1. A depth to the

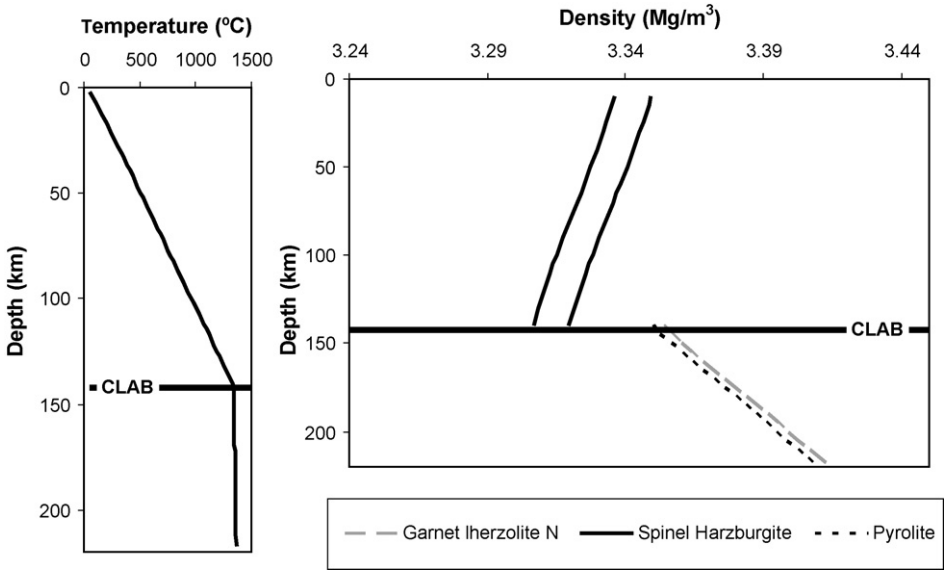

Fig. 6. Left: temperature gradient computed for the continental plate using as input the average heat-flow density calculated for the Subandean Ranges-Chaco region (40 mW/m^2). A depth of approximately 140 km can be inferred for the lithosphere–asthenosphere boundary (CLAB). Right: density profiles calculated along such thermal gradient for spinel harzburgites, garnet lherzolite N and pyrolite of Hacker and Abers (2004). The depth of the continental lithosphere–asthenosphere boundary (CLAB) is also shown.

oceanic lithosphere–asthenosphere boundary (OLAB) of approximately 80 km was determined by the intersection of the plate cooling model gradient with a mantle adiabat described by a potential temperature of 1300 °C and a gradient of 0.30 °C/km (Fig. 4). We calculated density profiles along such thermal gradient for spinel harzburgites and spinel and garnet lherzolites ("hzG", "hzH", "lherzolite", "lherzolite, basal", "pyrolite" and "garnet lherzolite N" of Hacker and Abers, 2004) (Fig. 4). Spinel harzburgites would represent depleted continental lithosphere, while garnet lherzolites would characterize fertile asthenosphere. The oceanic lithosphere would have an intermediate mineralogical composition between these end members (e.g. Lee et al., 2005; Tassara et al., 2006). From these density profiles we calculated average densities for the lithosphere (3.29 Mg/m^3) and the asthenosphere (3.35 Mg/m^3) (Fig. 3, Table 1):

$$\bar{\rho} = \frac{\sum_{i=1}^{n} \rho_i}{n} \quad \text{with} \quad \rho_i = \frac{1}{A-B} \int_A^B \rho(z) dz \tag{1}$$

with $\rho(z)$ being the density variation with depth. In the case of the lithosphere A and B are the depth to the OLAB (80 km) and to the Moho (10 km), respectively; while in the case of the asthenosphere A and B are 220 km (maximum depth modelled) and the depth to the OLAB (80 km), respectively.

We also calculated density profiles (Fig. 5) for an unmetamorphosed mid-ocean ridge basalt (MORB) and a fresh gabbro (both anhydrous), and for a fully hydrated basalt (zeolite metamorphic facies, 7.3% H_2O) and a partially hydrated basalt (prehnite-pumpellyite metamorphic facies, 4.5% H_2O) according to the mineralogical compositions proposed by Hacker et al. (2003) and the calculated temperature (Fig. 4) and lithostatic pressure gradients. The density of 2.9 Mg/m^3 selected for the oceanic crust (Fig. 3, Table 1) corresponds to a crust composed of 40% of fresh anhydrous basalts/grabbros and 60% of fully hydrated basalts. Such a composition of the crust would be in accordance with the existence of important amounts of hydrothermal alteration by seawater circulation (Stern, 2002).

The thermal structure of the Andean subduction zone and the metamorphic transformations underwent by the Nazca slab with depth are only partially known (e.g. Springer, 1999; Yuan et al., 2000). Yuan et al. (2000) used *P* to *S* converted teleseismic waves to image the deep structure of the subducted Nazca plate in the Central Andes. They suggested that gabbro to eclogite transformation in most of the subducted oceanic crust was completed at a depth of about 120 km. Taking into account the incomplete knowledge of the mineralogical changes underwent by the Nazca slab during subduction and that eclogite is the thermodynamically stable modification of mafic rocks at depth greater than 80 km (Peacock, 1993), we considered that eclogitization occurs at depths between ~60 km and 80 km producing a density increase, which would result in negative buoyancy (Stern, 2004; Hacker et al., 2003). We made density calculations for different mineral modes for MORB at various metamorphic facies, according to the phase diagram and mineralogical compositions proposed by Hacker et al. (2003). The depth stability range of each metamorphic facies was determined from the calculated temperature (Fig. 4) and lithostatic pressure gradients. Between approximately 15 km and 20 km

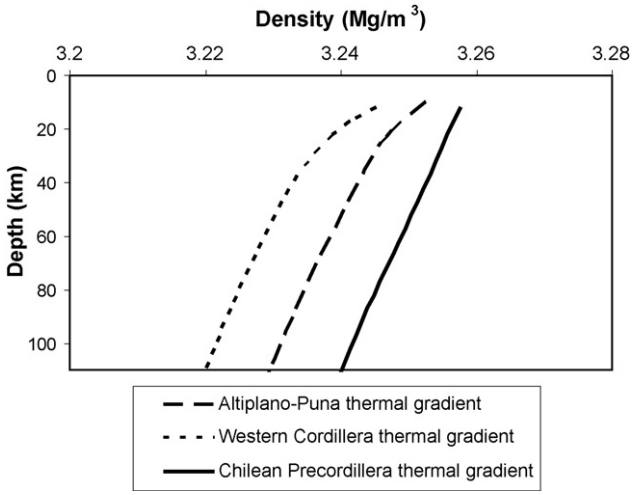

Fig. 7. Density profiles obtained for a chlorite harzburgite (Hacker et al., 2003), according to the Altiplano-Puna (AP), Western Cordillera (WC) and Chilean Precordillera (PC) thermal gradients.

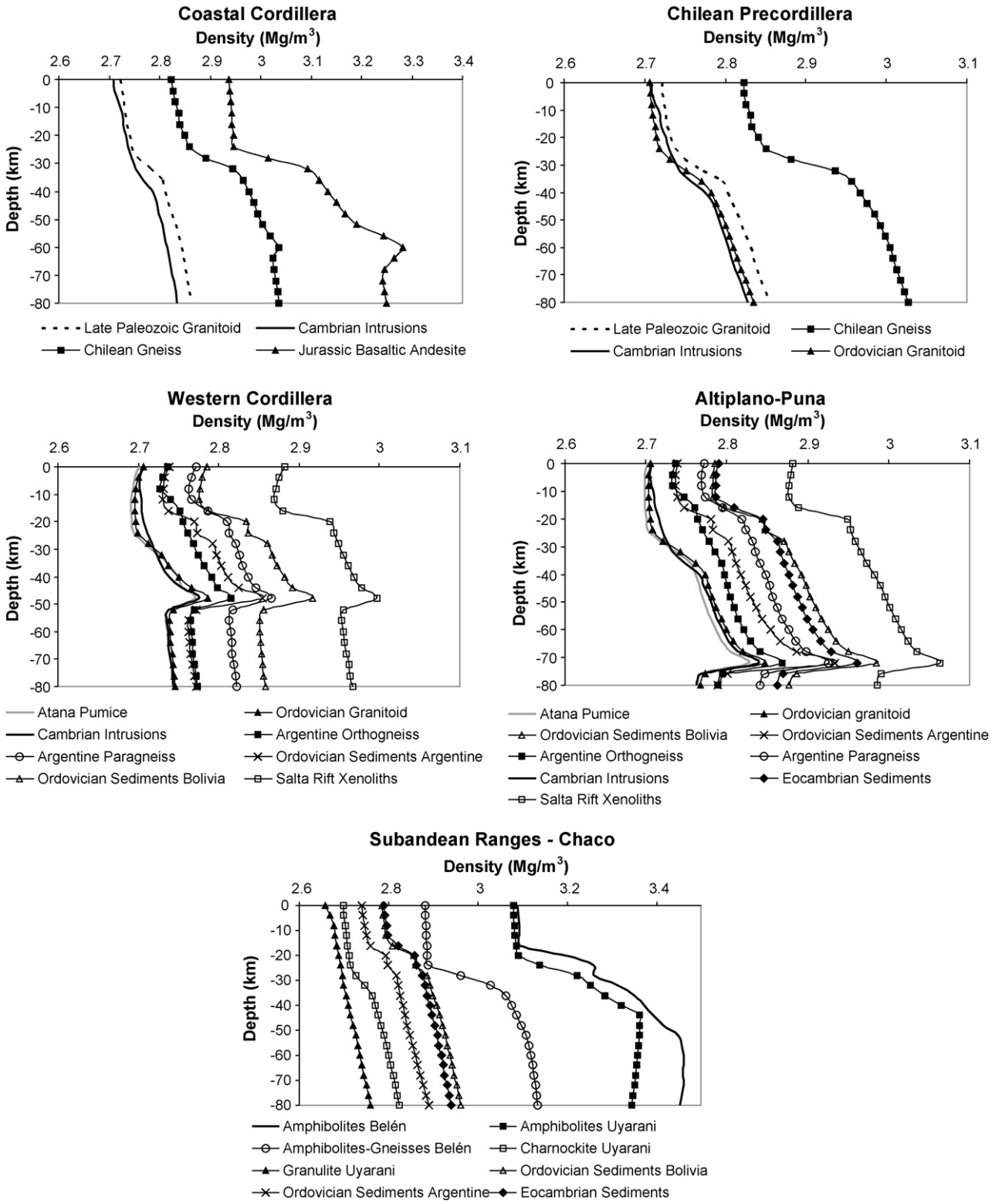

Fig. 8. Density profiles obtained for the different rock units composing the continental crust corresponding to the different Central Andean morphotectonic units.

depth greenschist metamorphism would occur, between 20 km and 30 km depth epidote amphibolite facies would be stable, between 30 km and 50 km depth garnet amphibolite metamorphism would take place, between 50 km and 65 km depth garnet granulite facies would be stable, and at greater depths eclogitization would be the dominant transformation. We obtained density profiles for the above-mentioned metamorphic facies, considering that the original MORB was fully metamorphosed. Trying to reproduce these mineralogical transformations in our model, we assumed that the oceanic crust of the slab has a density of 3.05 Mg/m^3 between approximately 35 km and (65–80) km depth, and a density of 3.45 Mg/m^3 between (65–80) km and 220 km depth (Fig. 3, Table 1). We considered that the oceanic lithosphere also increases its density with depth. We assigned it a density of 3.38 Mg/m^3 between

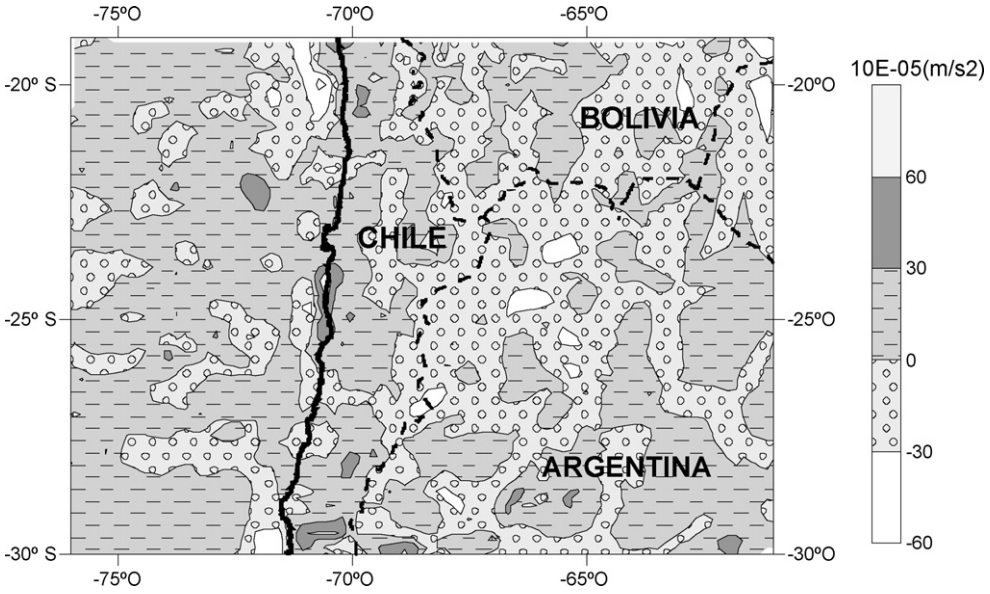

Fig. 9. Residual Bouguer anomaly generated by the final model. The residual was calculated as the difference between observed and calculated Bouguer anomaly. Black line: coast line. Dashed black lines: political borders.

approximately 50 km and 220 km depth (Fig. 3, Table 1). Without a better understanding of the thermal structure along the Andean subduction zone, the density structure of the slab proposed here should be considered as a rough estimation.

3.6.2. Continental plate

To calculate the densities of the continental lithosphere and asthenosphere we used the Excel Macro of Hacker and Abers (2004), modified by Tassara (2006). The temperature gradient was defined by a conductive geotherm with radioactive heat production in the crust (Turcotte and Schubert, 2002). To compute the temperature gradient we considered a surface temperature of 25 °C, a thermal conductivity for the lithospheric mantle of 3.3 W/m°C (Springer, 1999), a length scale for the decrease in radiogenic heat production with depth of 10 km (Turcotte and Schubert, 2002) and a mantle (reduced) heat-flow to the base of the lithosphere of 30 mW/m^2 (Turcotte and Schubert, 2002). Using this approach, the thermal gradient of the continental lithosphere is defined by the surface heat-flow density. As in the case of the oceanic area, the depth to the CLAB is determined by the intersection of the conductive gradient with a mantle adiabat described by a potential temperature of 1300 °C and a gradient of 0.30 °C/km. We compiled surface heat-flow density data for the Central Andes (Henry and Pollack, 1988; Hamza and Muñoz, 1996; Springer and Förster, 1998; Hamza et al., 2005), and calculated average values for different morphotectonic units: Coastal Cordillera: 24 mW/m^2, Chilean Precordillera: 51 mW/m^2, Western Cordillera: 110 mW/m^2, Altiplano-Puna: 82 mW/m^2 and Subandean Ranges-Chaco: 40 mW/m^2. We used these average values to generate thermal gradients for each morphotectonic unit. A depth of approximately 142 km was determined for the CLAB below the Subandean–Chaco region. We calculated density profiles along the Subandean Ranges-Chaco thermal gradient for spinel harzburgites and garnet lherzolites ("hzG", "hzH", "pyrolite" and "garnet lherzolite N" of Hacker and Abers, 2004) (Fig. 6). Spinel harzburgites would represent depleted continental lithosphere, while garnet lherzolites would characterize fertile asthenosphere. From these density profiles, average densities for the lithosphere (3.34 Mg/m^3) and the asthenosphere (3.37 Mg/m^3) (Fig. 3, Table 1) were calculated using equation (1). In the case of the lithosphere, A and B (Eq. (1)) are the depth to the CLAB (140 km) and to the Moho (40 km), respectively; while in the case of the asthenosphere A and B (Eq. (1)) are 220 km (maximum depth modelled) and the depth to the CLAB (140 km), respectively. To the west of the Subandean–Chaco region the depth and the geometry of the CLAB change along the model according to the additional constraining geophysical data (see Section 3.5.2), and in concert with the observations of Withman et al. (1996).

A significant amount of asthenospheric wedge melting, triggered by dehydration of the subducting slab, occurred during the Central Andes evolution (e.g. Coira and Kay, 1993; Kay et al., 1999; de Silva et al., 2006; Kay et al., 2008) probably resulting in a relatively depleted mantle wedge. Therefore, to gain insight into the possible density of the asthenospheric wedge we computed the densities corresponding to a chlorite harzburgite (1.4% H_2O) (Hacker et al., 2003) according to the Altiplano-Puna, Western Cordillera and Chilean Precordillera thermal gradients (Fig. 7). For the average range of pressures (1.5–3 GPa) and temperatures (600–900 °C) expected for the modelled asthenospheric wedge body, chlorite harzburgites are the stable phases (Hacker et al., 2003). We assigned an average density of 3.25 Mg/m^3 for the asthenospheric wedge (Fig. 3, Table 1). It is important to mention that the geometry of the asthenospheric wedge changes in N–S direction, being constrained by travel time and attenuation tomography sections. Moreover, in our model there are compositional and thermal differences between the lithosphere and the asthenosphere. The lithosphere is considered to be composed by spinel harzburgites, whose densities decrease along a conductive thermal gradient towards the CLAB. On the other hand, the asthenosphere is considered to be composed by garnet lherzolites, whose densities increase along an adiabatic gradient (Fig. 6). Consequently, the asthenosphere has higher average density than the lithosphere, contrary to the idea derived from the presence of a low-velocity zone below some continental plates (e.g. Turcotte and Schubert, 2002). However, the density of 3.25 Mg/m^3 assigned to the asthenospheric wedge below the Western Cordillera and the Altiplano-Puna, where heat-flow is higher than 80 mW/m^2, is lower than the density of the reference mantle. Such negative density contrast can be linked with the mantle low-velocity zone (Tassara et al., 2006).

It is expected that the westernmost part of the upper continental mantle (below de Coastal Cordillera and the western Chilean

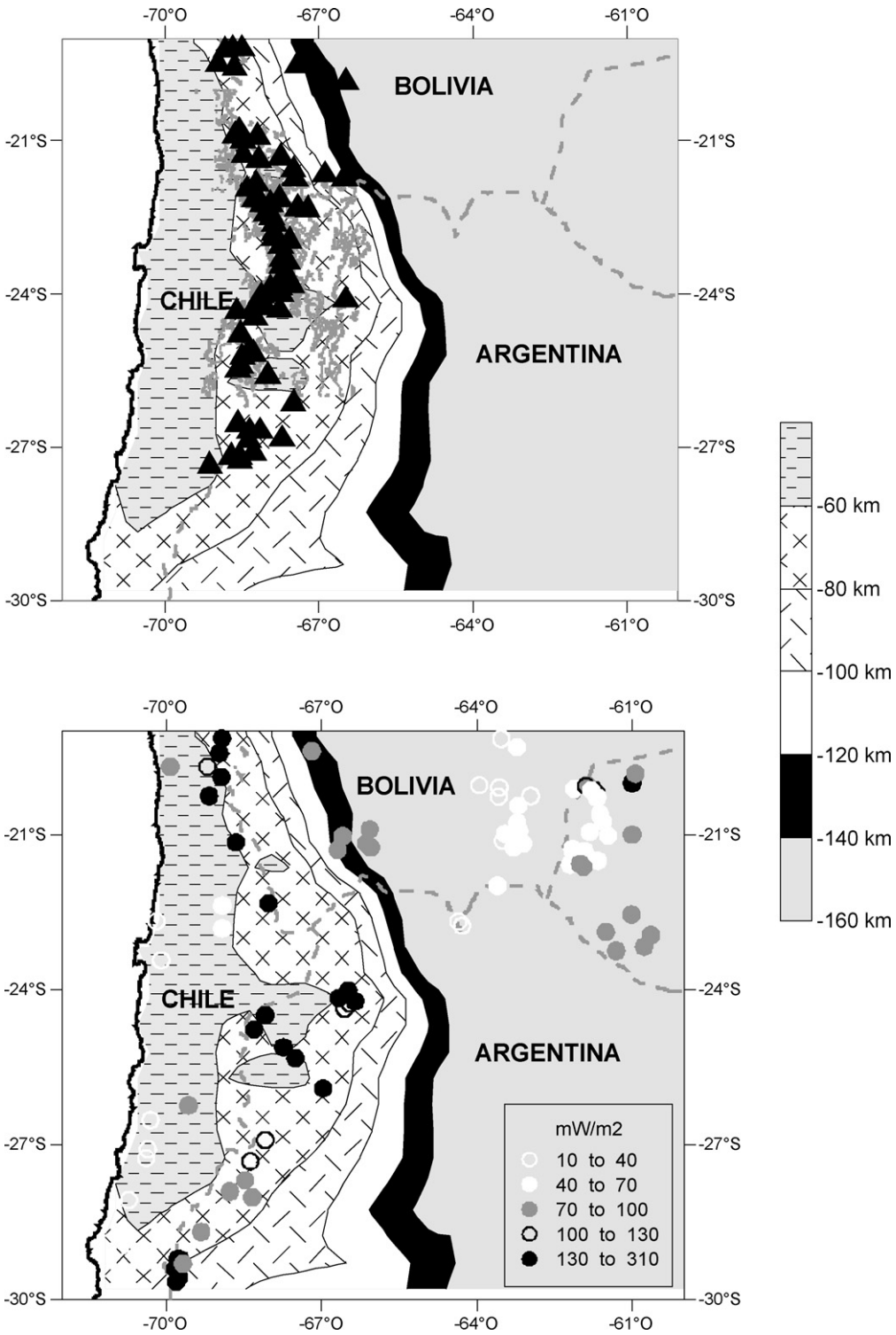

Fig. 10. Contour map of the modelled continental lithosphere–asthenosphere boundary (CLAB) depth. Top: black triangles: active volcanoes from the Smithsonian Institute (www.volcano.si.edu/gvp/world), grey line: Altiplano-Puna Volcanic Complex, dashed grey line: political borders, black line: coast line. Bottom: circles: heat-flow values, dashed grey line: political borders, black line: coast line.

Precordillera) would contain important amounts of hydrated serpentinized material. Wigger et al. (1994) detected a low-velocity zone (average velocity 6.4–6.6 km/s) between 15 km and 45 km depth below the Coastal Cordillera and the western Chilean Precordillera along a cross-section at 21.25°S. They proposed that uppermost ultrabasic Jurassic-Cretaceous mantle was partially serpentinized by the introduction of water from the descending slab, inducing the reduction in velocities. Wigger et al. (1994) also suggested an alternative interpretation of this low-velocity zone, considering that the Jurassic arc developed upon a continental crust with the forearc west of the actual Coastal Cordillera. These authors concluded that 200 km of such forearc was consumed by tectonic erosion. Such crustal material could have formed or contributed together with serpentinization to the generation of the low-velocity zone. Wigger et al. (1994) noted that magmatic addition should also be taken into account. They proposed that a

combination of all these processes should be considered to explain the low-velocity zone. Other authors have also suggested the existence of serpentinization in the mantle wedge below the Andean forearc (e.g. Graeber and Asch, 1999; Schmitz et al., 1999; Giese et al., 1999; Sick et al., 2006; Tassara et al., 2006). Graeber and Asch (1999) considered that the presence of serpentinite below the Coastal Cordillera at a depth of 50 km could account for the lowered P velocities and the very high v_p/v_s ratio documented along 22.75°S. Schmitz et al. (1999) observed a depth interval between 30 km and 50 km below the Coastal Cordillera and between 40 km and 65 km below the Chilean Precordillera along a cross-section at 23.0–23.5°S characterized by high v_p/v_s values, indicating the existence of hydrated mantle rocks as serpentinites. These authors also detected a prominent interface located at 50–65 km depth in the Chilean Precordillera. They interpreted that this boundary could represent the transition zone between the serpentinites and amphibole-bearing peridotites in the hydrated mantle wedge. Giese et al. (1999) noted that the temperatures in the mantle wedge are below 600 °C in the Andean forearc region and thus in the stability field of serpentinite, but that above a temperature of 700 °C and a depth of >50–60 km amphibole-bearing peridotite is stable. Serpentinites show distinctly lower densities (~2.9–3.0 Mg/m^3) than amphibole-bearing peridotites (>3.1 Mg/m^3) and peridotites (>3.3 Mg/m^3) (Giese et al., 1999). Giese et al. (1999) proposed the existence of mantle serpentinites between 15 km and 50 km depth below the Coastal Cordillera along 21°S. Sick et al. (2006) showed the presence of a hydrated mantle wedge between 20 km and 40 km depth below the Coastal Cordillera and between 30 km and 50 km depth below the Chilean Precordillera, using wide-angle seismics along a cross-section at 23.25°S. In their 3D gravity modelling Tassara et al. (2006) considered the existence of serpentinized harzburgites between 30 km and 100 km depth in the Andean mantle forearc. The presence of serpentinized mantle forearc in subduction zones is ubiquitous (Hyndman and Peacock, 2003). Kamiya and Kobayashi (2000) detected sismologically the presence of serpentinized peridotite above the subducting plate in central Japan. Their models show low-velocity anomalies, which they attributed to the existence of serpentinized peridotites in the mantle wedge at depths of 20–45 km. Bostock et al. (2002) also identified the presence of a serpentinized mantle forearc between 30 km and 60 km depth in the southern Cascadia subduction zone using scattered teleseismic waves. Considering all the information mentioned above, we included in our model two bodies with the aim of representing mantle wedge serpentinization, crustal material added by tectonic erosion and magmatic addition (Wigger et al., 1994) (Fig. 3). Taking into account that the percentage of serpentinization of the fore arc mantle that can be deduced from seismic velocities (Carlson and Miller, 2003) would be of about 35–45% (with ~5–6% H_2O), we calculated density profiles for chlorite serpentine wehrlite (7.5% H_2O, 29% serpentine), depleted chlorite serpentine wehrlite (6.5% H_2O, 39% serpentine) and serpentine chlorite dunite (6.2% H_2O, 40% serpentine) (Hacker et al., 2003) considering the Coastal Cordillera and the Chilean Precordillera geotherms. From the obtained results we calculated average densities of 2.92 Mg/m^3 and 2.93 Mg/m^3 for this part of the upper mantle (Fig. 3, Table 1). These results coincide with the values proposed by Giese et al. (1999). However, Yuan et al. (2000) interpreted the low-velocity zone mentioned above as being the crust of the downgoing Nazca plate. In this case, given the similar densities between serpentinite (2.92–2.93 Mg/m^3) and oceanic basalts/gabbros (2.90 Mg/m^3) (Fig. 3, Table 1), the fit between modelled and measured gravity anomalies would not be significantly affected. Furthermore, our density model could properly represent both situations.

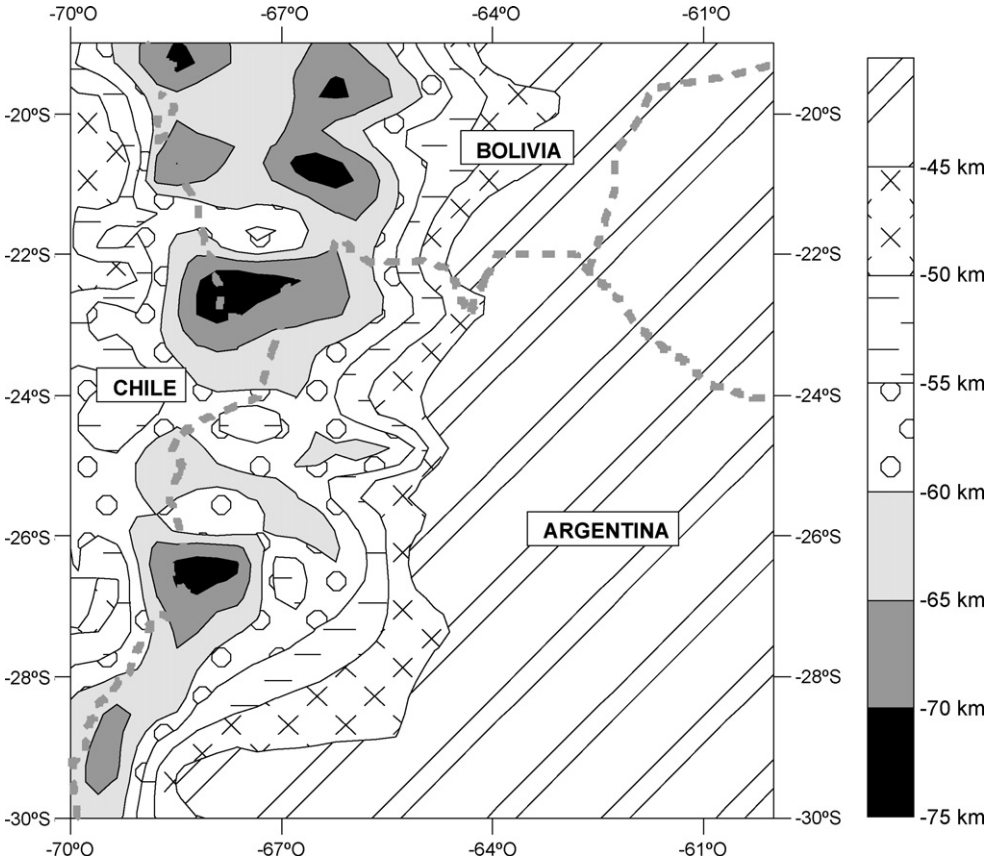

Fig. 11. Contour map of the modelled continental Moho depth. Dashed grey lines: political borders.

The Excel Macro of Hacker and Abers (2004) was designed to investigate properties of mafic and ultramafic rocks at high temperature and pressure. Therefore, it cannot be applied to the study of the continental crust. To constrain the densities of the continental crust we used an updated version of the algorithm of Sobolev and Babeyko (1994) (Sobolev and Babeyko, personal communication). This code permits the calculation of density profiles along temperature–pressure gradients from the major element chemical composition of rocks, imposing a kinetic barrier of 700 °C as the minimum equilibrium temperature allowed. To compute the pressure and temperature gradients for the different morphotectonic units, the above-mentioned heat-flow averages, a thermal conductivity for the continental crust of 2.5 W/m°C (Springer, 1999) and an average density of 2.9 Mg/m^3 were used. We compiled major element compositions of rocks from the modelled area published by Lucassen et al. (1999), Wörner et al. (2000) and Lucassen et al. (2001). Lucassen et al. (1999) investigated granulite and peridotitic xenoliths from the Salta Rift System. These xenoliths are the only directly available samples from the lower crust of the Central Andes. Most of them have a granitoid composition, mafic xenoliths are exceedingly rare. Wörner et al. (2000) presented geochemical, petrologic and geochronologic data from the Proterozoic metamorphic basement exposures at Belén in northern Chile and the Cerro Uyarani on the Bolivian Altiplano. Lucassen et al. (2002) considered that such basement corresponds to the Brazilian shield. Lucassen et al. (2001) compiled average major element compositions of various rock units from Central Andes: Atana Pumice, Late Palaeozoic granitoids, Ordovician granitoids, Ordovician sediments, Chilean gneisses, Argentine gneisses, Cambrian intrusions, Eocambrian sediments and Jurassic basaltic andesites from the Coastal Cordillera. We calculated density profiles for the different rock units cropping out in each morphotectonic unit according to the corresponding thermal gradients (Fig. 8). Regarding the Cretaceous-Tertiary sedimentary sections of the Altiplano-Puna and the Subandean Ranges-Chaco, some density logs from oil companies are available. Gangui (1998) extracted density information from one well density log in northern Argentine Puna. He computed a weighted average density for depths ranging between 200 km and 1365 m of 2.49 Mg/m^3. According to these results, we allocated the densities summarized in Table 1 and displayed in Fig. 3 to the bodies composing our model. The selection of such values is in general agreement with the densities proposed for the study area by the global crustal model CRUST 2.0 (http://mahi.ucsd.edu/Gabi/rem.html, Bassin et al., 2000). It is important to mention, that such model was developed on the basis of a detailed compilation of seismic refraction measurements. The densities presented in the global model were estimated using empirical v_p—density relationships (Mooney et al., 1998). Therefore, they constitute an independent constraint on our density calculations. Moreover, the densities computed here for the lower crust (Table 1) also coincide with the ones calculated by Lucassen et al. (2001). They obtained a value of 2.95 Mg/m^3, considering a felsic composition for the whole crust (equal to the one of the Chilean gneisses). They also estimated that the density of the Coastal Cordillera middle-lower crust would be well above 3.0 Mg/m^3, using as input the chemical composition of the Jurassic basaltic andesites.

3.7. Decision-making process, model precision and model sensitivity

Trying to reduce the ambiguity and the uncertainty inherent to the gravimetric method, we decided not to vary certain aspects of the density structure during the forward modelling. Thereby, the densities assigned to each one of the modelled bodies (according to the calculations explained above, see Section 3.6) were considered fixed and were not changed to obtain a better fit of the measured and calculated anomalies. Likewise, the geometries defined by the additional data included in the model (see Section 3.5) were not modified. Only those boundaries, whose geometries were not constrained by other data, were modified.

The forward modelled 3D density structure thoroughly reproduces the measured gravity field. The residual Bouguer anomaly depicts the differences between measured and modelled anomalies. Only less than ~15% of the study area presents residual anomalies greater than 30×10^{-05} m/s^2 (Fig. 9). Such anomalies are of very short wave length and are not systematically distributed in the map. Residual anomaly values are tightly concentrated around 0 m/s^2, with a standard deviation of 16.47×10^{-05} m/s^2. These results suggest that our model satisfactorily represents the density structure of the Central Andes.

We used the facilities of IGMAS modelling software to test the sensitivity of the model to changes in the densities allocated to the forming bodies. Table 1 shows the percentage variation of density of each modelled body that would produce a variation of the calculated Bouguer anomaly of $\pm 20 \times 10^{-05}$ m/s^2. Tolerable density variations increase with depth and decrease with rising total mass of the corresponding bodies. It can be observed that tolerable variations range between 0.15% and 5.22% (Table 1), with an average of 1.5%. The uncertainties related to the chemical and mineralogical compositions, the thermal and lithostatic pressure gradients, the seismic velocities and the algorithms available to calculate densities, are much higher than the tolerable density variations of our model.

4. Description and discussion of Results

Fig. 10 shows a contour map of the CLAB. Heat-flow data (Henry and Pollack, 1988; Hamza and Muñoz, 1996; Springer and Förster, 1998; Hamza et al., 2005), the location of active volcanoes and the approximate extent of the Altiplano-Puna Volcanic Complex (APVC) are also depicted. The APVC is a late Miocene to Recent ignimbrite "flare-up" that covers ~50000 km^2 (Beck and Zandt, 2002). There is a remarkable spatial coincidence between the ignimbritic cover, the occurrence of heat-flow values higher than 100 mW/m^2 in the Puna and a widening of the region where the top of the asthenosphere is at depths between 60 km and 80 km. Such region also coincides with the approximate extent of the mid-crustal Altiplano-Puna magma body (Zandt et al., 2003). Furthermore, modern volcanoes approximately follow the 60 km depth contour line. South of ~27°S no active volcanism is reported, in correlation with a notable deepening of the CLAB and the flattening of the subducted slab. In addition, the existence of a particularly deeper CLAB below the Altiplano than below the Puna is clearly observed. Withman et al. (1996) suggested that the transition between the ~4 km high Altiplano and the ~5 km high Puna could be associated with a rapid southward thinning of the lithosphere, in coincidence with our results.

Fig. 11 shows contour lines of the modelled Moho geometry. It can be seen that the Central Andes has a thick crustal root, which mimics the topography. The modelled Moho beneath the Salar de Atacama basin is deeper than expected, considering the basin's low elevation. This situation was noted also by other authors (Wigger et al., 1994; Schurr and Rietbrock, 2004). Modelled crustal thickness reaches maximum values of 77 km beneath the Altiplano and northern Puna (north of 24°S), while the southern Puna (south of 24°S) is underlain by a thinner crust up to 66 km thick (Fig. 11). Average crustal thickness below the southern Puna is approximately 10 km lower than below the Altiplano (north of 22°S) and the northern Puna (22–24°S). However, the topography in the southern Puna is as high as in the northern Puna, and it is higher than in the Altiplano.

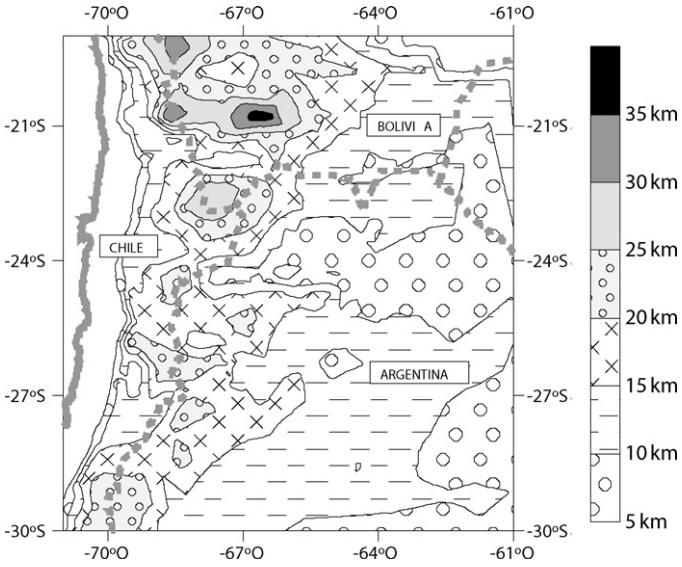

Fig. 12. Contour map of the modelled lower crustal thickness. Dashed grey lines: political borders, grey line: coast line.

It was proposed by Yuan et al. (2002) that the Puna could be compensated by a thermal anomaly related to shallow asthenosphere. Such interpretation would be supported by the geometry obtained in our model for the top of the asthenosphere (Fig. 10). Taking into account these results, we prepared a contour map of the modelled lower crustal thickness (density: 3.0–3.04 Mg/m^3) (Fig. 12). It can be observed that while lower crustal thickness reaches values of up to 38 km below the Altiplano (north of 22°S) (with average values of ~30 km), it decreases to the south, reaching values of less than ~25 km in the northern Puna (22–24°S) and of less than ~20 km in the southern Puna (south of 24°S). Yuan et al. (2002) proposed the existence of mafic lower crust (density ~ 3.2 Mg/m^3) below the Altiplano and its absence below the southern Puna. The presence of thinner lower crust below the southern Puna, supports the occurrence of delamination proposed by other authors (Kay and Kay, 1993; Kay et al., 1994; Allmendinger et al., 1997) and the existence of shallower asthenosphere.

Following the approach of Schilling and Partzsch (2001) we try to estimate the possible amount of partial melting that occurs in the Andean low-velocity zone. We use as input data the densities assigned in our model to the Altiplano-Puna middle crust and to the Altiplano-Puna partial melting zone (Table 1). If we consider a density of 2.43 Mg/m^3 for the melt, we obtain 9% of partial melting. Such melt density was used by Babeyko et al. (2002) to perform a 2D thermo-mechanical modelling, with the aim of studying possible mechanisms for generating large-scale crustal magmas in the Altiplano-Puna region. The value of 9% resulting from our estimation, agrees with the ones modelled by Babeyko et al. (2002). In their preferred model ("weak" felsic crust) the percentage of partial melting between ~15 km and 35 km depth is of 5–12%. Other authors suggested percentages of partial melting: Schmitz et al. (1997): 15–20%, Schilling et al. (1997): 14–27%, Schilling and Partzsch (2001): 20%, Beck and Zandt (2002): 5–10%.

In order to further investigate the Central Andean crustal structure, the residual gravity anomaly is calculated. Fig. 13 presents the residual gravity field obtained by subtracting the effect of the modelled subducted Nazca plate (assuming a density contrast of 0.03 Mg/m^3) and the effect of the modelled Moho (assuming a density contrast of −0.5 Mg/m^3) from the Bouguer anomaly. Positive residual anomalies larger than 50×10^{-05} m/s^2 are observed in the forearc, the Salar de Atacama basin and the Bolivian Eastern Altiplano-Eastern Cordillera. Negative values of less than -50×10^{-05} m/s^2 can be seen along the recent volcanic arc (Western Cordillera) and in the southern Puna (south of 24°S). Regarding the Salar de Atacama basin, the observed difference could be caused by the Atacama block. The Atacama block is rheologically strong (with high Q_p and ν_p values) (Schurr and Rietbrock, 2004) and has a positive density contrast. In the case of the fore arc, the positive residual anomaly could be related to the presence of uplifted Jurassic batholiths intruded into La Negra Formation (modelled with a density contrast of 2.73 Mg/m^3) (Fig. 3) (Götze and Kirchner, 1997), and to a zone of high densities (>3.0 Mg/m^3) and velocities (7.2–7.4 km/s) at 20–25 km depth (Fig. 3) (interpreted as the lower crust of the Jurassic magmatic arc) (Wigger et al., 1994; Schmitz et al., 1999). It may be speculated that the presence of thicker mafic lower crust below the Altiplano and western Bolivian Eastern Cordillera (Yuan et al., 2002) (Fig. 12) could be responsible of the positive residuals detected. On the other hand, the negative anomalies observed in the southern Puna would be in agreement with the existence of thinner or absent mafic lower crust (Yuan et al., 2002) (Fig. 12) due to delamination (Kay and Kay, 1993; Allmendinger et al., 1997). The negative values along the recent magmatic arc would point to partial melting and low-density volcanic rocks. The existence of partial melts in the Central Andes is well constrained as was previously mentioned (Schilling and Partzsch, 2001; Schilling et al., 1997).

Isostatic gravity fields are obtained by subtracting the effect of the modelled subducted Nazca plate (assuming a density contrast of 0.03 Mg/m^3) and the effect of different isostatic Mohos (assuming a density contrast of −0.5 Mg/m^3) from the Bouguer anomaly. In a first approach, we computed the isostatic compensation of the topography (GTOPO30: http://edcdaac.usgs.gov/gtopo30/gtopo30.asp; density: 2.67 Mg/m^3) assuming a normal

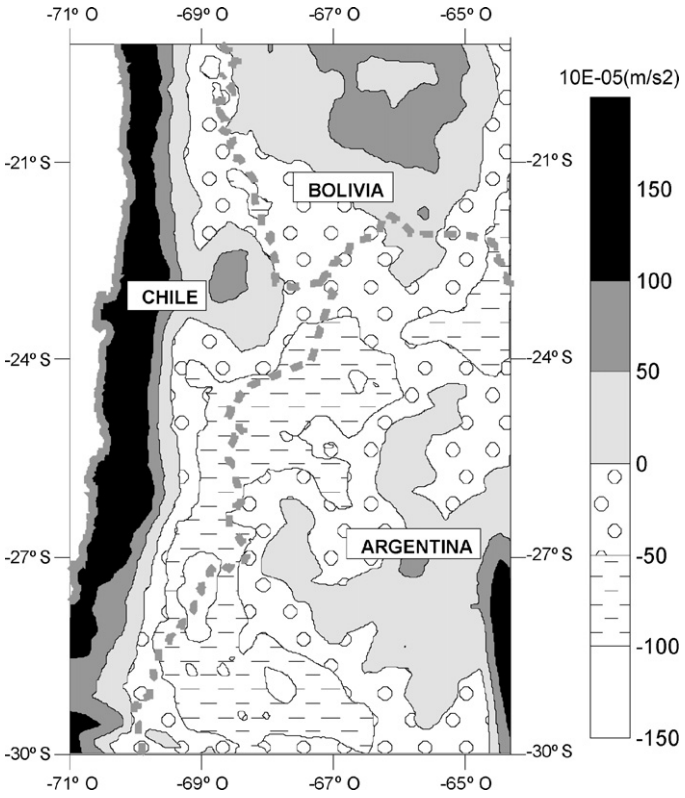

Fig. 13. Residual gravity field obtained by subtracting the gravimetric effects of the modelled subducted plate (assuming a density contrast of 0.03 Mg/m^3) and of the modelled Moho (assuming a density contrast of −0.5 Mg/m^3) from the Bouguer anomaly. Dashed grey lines: political borders, grey line: coast line.

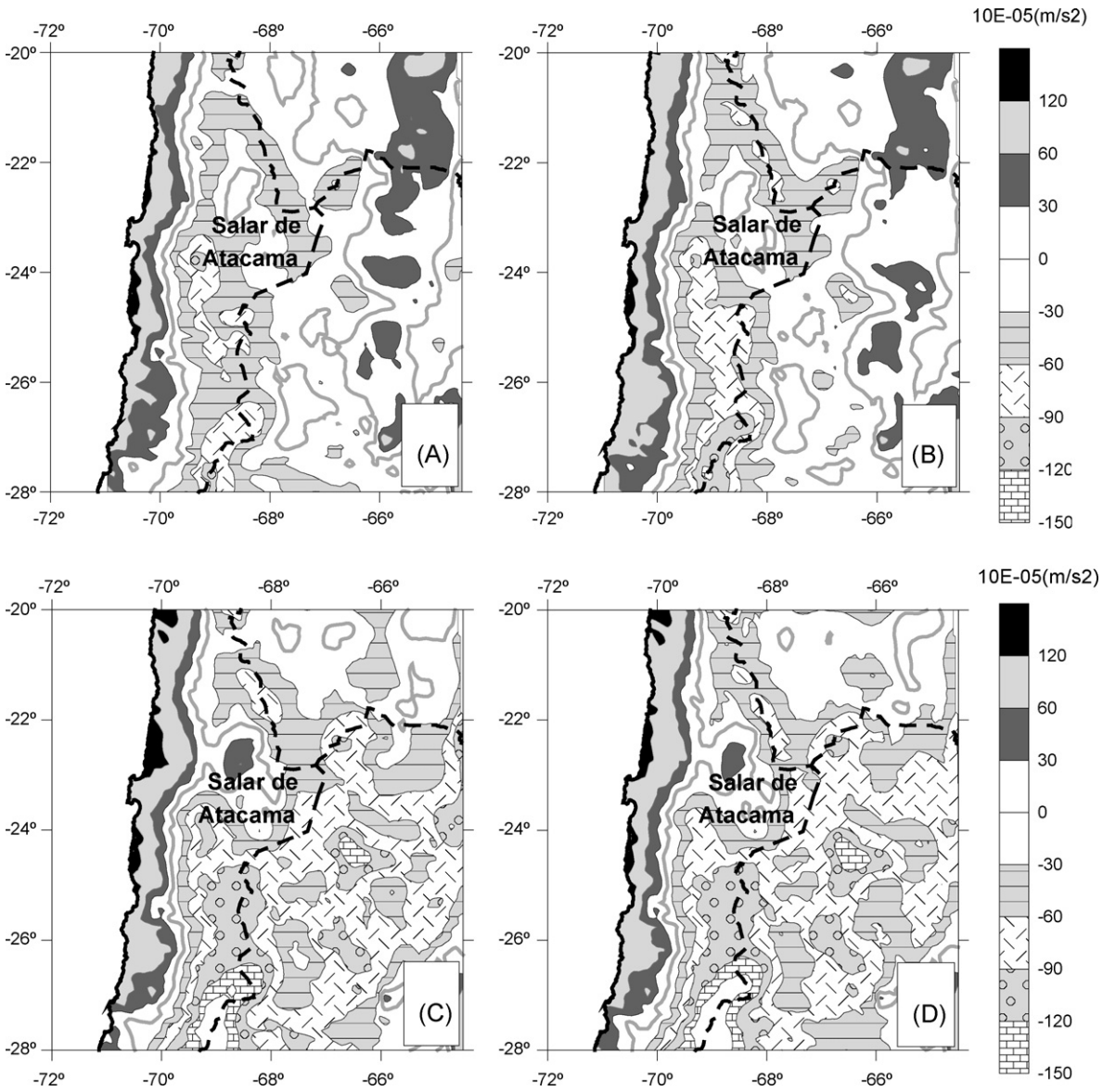

Fig. 14. Isostatic gravity fields. A: assuming Airy model, considering only surface loads, B: assuming Vening-Meinesz model, considering only surface loads, C: assuming Airy model, considering surface and internal loads, D: assuming Vening-Meinesz model, considering surface and internal loads. Dashed black lines: political borders; black line: coast line; thick grey bold line: 0 m/s^2 contour.

crustal thickness of 40 km and applying: (1) Airy compensation and (2) the model of Vening-Meinesz. In a second approach we computed isostatic compensation using the same inputs and assuming Airy and Vening-Meinesz models, but including also internal loads. Internal (subsurface) loads result from the irregular density distribution within the lithosphere. The internal loads (L) are directly calculated from our 3D density model in vertical columns with reference to a normal crust using:

$$L = \sum_{i=1}^{n} h_i(\rho_i - \rho_c) \quad (2)$$

where h_i is thickness and ρ_i is density of the i-th layer and ρ_c the density of the reference crust, in this case taken as 2.88 Mg/m^3. Fig. 14a–d show the different isostatic anomalies calculated. Regarding Vening-Meinesz model, recent studies have shown that the elastic thickness (Te) varies along the Central Andes (e.g. Tassara et al., 2007; Pérez-Gussinyé et al., 2008, 2009). Tassara et al. (2007) used a wavelet formulation of the classical spectral isostatic analysis to invert satellite-derived gravity and topography/bathymetry for Te over South America. Pérez-Gussinyé et al. (2008, 2009) obtained Te estimates along the Andes from multitaper coherence of Bouguer gravity and topography data. According to the calculations of Tassara et al. (2007), ~80% of the area mapped in Fig. 14 is characterized by Te values that range between ~8 km and 20 km. Estimates by Pérez-Gussinyé et al. (2008, 2009) show that Te is ~20 km over ~80% of the studied area. Maximum Te values obtained by Tassara et al. (2007) and Pérez-Gussinyé et al. (2008, 2009) for the area considered in our calculations (Fig. 14) are of ~40 km. In light of this and given that Te is a proxy for rigidity, we used a constant rigidity of 3.5×10^{22} Nm (which corresponds to a Te of ~18 km). The main differences between the isostatic anomalies obtained considering internal loads (IAIL) (Airy and Vening-Meinesz models) (Fig. 14c and d) and those calculated taking into account only surface loads (IA) (Fig. 14a and b), are that the first ones show values ranging between −30 m/s^2 and 30×10^{-05} m/s^2 below the eastern Altiplano-western Bolivian Eastern Cordillera (north of 22°S), strong negative values below the entire Puna (south of 22°S) and positive values beneath the Salar de Atacama basin. The absence of strong positive anomalies in the

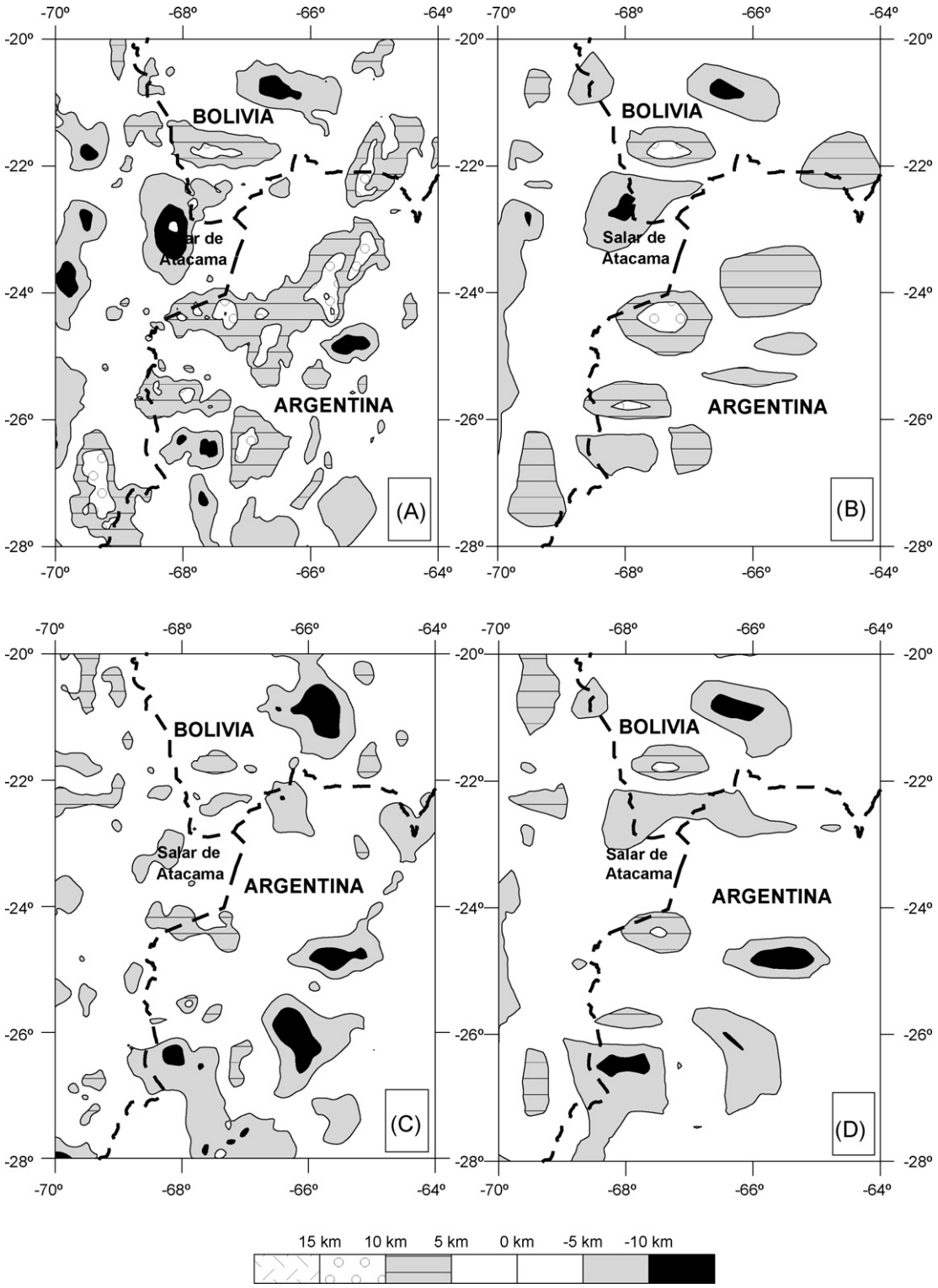

Fig. 15. Depth differences between the modelled Moho and the isostatic Mohos, obtained by subtracting the isostatic Moho depths from the modelled Moho depths. A: assuming Airy model, considering only surface loads, B: assuming Vening-Meinesz model, considering only surface loads, C: assuming Airy model, considering surface and internal loads, D: assuming Vening-Meinesz model, considering surface and internal loads. Dashed black lines: political borders.

eastern Altiplano-western Bolivian Eastern Cordillera in the IAIL supports the 3D density structure proposed in our model. The negative IAIL below the Puna would indicate a deficit of mass, which agrees with the presence of partial melting, the thermal state (very high heat-flow) and the felsic composition of the overthickened crust, with thinner lower crust than below the Altiplano (Lucassen et al., 2001). The positive density contrast of the strong and cold Atacama block is reflected in the positive anomaly observed in the Salar de Atacama basin in the IAIL.

Fig. 15 shows the depth differences between the modelled Moho and the isostatic Mohos (Airy and Vening-Meinesz models) obtained by subtracting the isostatic Moho depths from the modelled Moho depths. The modelled Moho is deeper than the isostatic ones beneath the Salar de Atacama and the fore arc (Fig. 15a and

b), while it is shallower below the Puna (south of 22°S). Such differences decrease notably if we take into account internal loads in the calculation of the isostatic Mohos (Fig. 15c and d). This fact supports our proposed 3D density structure, in spite of the persistence of some differences (particularly below the Altiplano and the southeastern border of the Puna).

5. Conclusions

The 3D density model presented in this study summarizes and integrates a large amount of geologic, geophysical, petrologic and geochemical information. Therefore, the resulting geometries (Moho, lower crustal thickness, top of the asthenosphere, subducted slab) contain new information and present more detail than previous ones.

The analysis and interpretation of our model allowed us to arrive at the following observations and conclusions:

a) A remarkable spatial coincidence between the Altiplano-Puna Volcanic Complex and a region of thin lithosphere is observed. Such region also coincides with the approximate extent of the mid-crustal Altiplano-Puna magma body and with the occurrence of very high heat-flow values.
b) South of ~27°S no active volcanism is reported, in correlation with a notable deepening of the continental lithosphere–asthenosphere boundary.
c) Modelled crustal thickness reaches maximum values of 77 km beneath the Altiplano and northern Puna, while the southern Puna is underlain by a thinner crust up to 66 km thick.
d) It was estimated that ~9% of partial melting would occur in the Andean low-velocity zone.
e) Lower crustal thickness decreases from north to south, being less than ~30 km below the Altiplano, less than ~25 km below the northern Puna and less than ~20 km below the southern Puna.
f) Positive residual anomalies observed in the Salar de Atacama basin coincide with the presence of the dense, cold and strong Atacama block.
g) Negative residual anomalies in the southern Puna, together with the existence of thinner crust, shallower asthenosphere and higher topography than in the Altiplano, would support the occurrence of lower crustal delamination.
h) The negative IAIL below the entire Puna (south of 22°S) would indicate a deficit of mass, which agrees with the existence of partial melting, high heat-flow and felsic composition of the overthickened crust with thinner lower crust than below the Altiplano (north of 22°S).
i) The fit between the modelled Moho and the isostatic Mohos calculated taking into account internal loads, supports our proposed 3D density structure.

Acknowledgements

This research was partially funded by Buenos Aires University (project UBACyT-X479 to C. Prezzi). Claudia B. Prezzi gratefully acknowledges the support of an Alexander von Humboldt Fellowship from the Alexander von Humboldt Foundation during which this work was carried out.

References

Allmendinger, R., Jordan, T., Kay, S., Isacks, B., 1997. The evolution of the Altiplano-Puna plateau of the Central Andes. Annual Review of Earth and Planetary Science 25, 39–174.
Allmendinger, R., Zapata, T., 2000. The footwall ramp of the Subandean decollement, northernmost Argentina, from extended correlation of seismic reflection data. Tectonophysics 321, 37–55.
ANCORP-Working-Group, 2003. Seismic imaging of a convergent continental margin and plateau in the Central Andes (Andean Continental Research Project 1996 (ANCORP 96)). Journal of Geophysical Research 108, doi:10.1029/2002JB001771.
Andersen, O., Knudsen, P., 1998. Global marine gravity field from the ERS-1 and GEOSAT geodetic mission altimetry. Journal of Geophysical Research 103, 8129–8137.
Babeyko, A., Sobolev, S., Trumbull, R., Oncken, O., Lavier, L., 2002. Numerical models of crustal scale convection and partial melting beneath the Altiplano-Puna plateau. Earth and Planetary Science Letters 199, 373–388.
Bassin, C., Laske, G., Masters, T., 2000. The current limits of resolution for surface wave tomography in North America. EOS Transactions AGU 81, F897.
Baumont, D., Paul, A., Zandt, G., Beck, S., 2001. Lateral variations of the Moho geometry beneath the Central Andes based on Pn travel time inversion and comparison with the receiver functions. Geophysical Research Letters 28, 1663–1666.
Beck, S., Zandt, G., 2002. The nature of orogenic crust in the Central Andes. Journal of Geophysical Research 107, doi:10.1029/2000JB000124.
Belmonte, A., 2002. Krustale Seismizität, Struktur und Rheologie der Oberplatte zwischen der Präkordillere und dem magmatischen Bogen in Nordchile (22°-24°S). Ph. D. Thesis. Freie Universität Berlin, Berlin.
Bock, G., Schurr, B., Asch, G., 2000. High-resolution image of the oceanic Moho in the subducting Nazca plate from P-S converted waves. Geophysical Research Letters 27, 3929–3932.
Booker, J., Favetto, A., Pomposiello, M., 2004. Low electrical resistivity associated with plunging of the Nazca flat slab beneath Argentina. Nature 429, 399–403.
Bostock, M., Hyndman, R., Rondenay, S., Peacock, S., 2002. An inverted continental Moho and serpentinization of the forearc mantle. Nature 417, 536–538.
Brasse, H., Lezaeta, P., Rath, V., Schwalenberg, K., Soyer, W., Haak, V., 2002. The Bolivian Altiplano conductivity anomaly. Journal of Geophysical Research 107, doi:10.1029/2001JB000391.
Breunig, M., Cremers, A., Götze, H.-J., Seidemann, R., Schmidt, S., Shumilov, S., Siehl, A., 2000. Geologic mapping based on 3D models using an interoperable GIS. Geo-Information-Systems Journal of Spatial Information and Decision Making 13, 12–18.
Carlson, R., Miller, D., 2003. Mantle wedge water contents estimated from seismic velocities in partially serpentinized peridotites. Geophysical Research Letters 30, doi:10.1029/2002GL016600.
Chmielowski, J., Zandt, G., Haberland, C., 1999. The Central Andean Altiplano-Puna magma body. Geophysical Research Letters 26, 783–786.
Christensen, N., Mooney, W., 1995. Seismic velocity structure and composition of the continental crust: a global view. Journal of Geophysical Research 100, 9761–9788.
Coira, B., Kay, S., 1993. Implications of Quaternary volcanism at Cerro Tuzgle for crustal and mantle evolution of the Puna Plateau, Central Andes. Contributions to Mineralogy and Petrology 113, 40–58.
Coira, B., Davidson, J., Mpodozis, C., Ramos, V., 1982. Tectonic and magmatic evolution of the Andes of northern Argentina and Chile. Earth Science Review 18, 303–332.
Cristallini, E., Cominguez, A., Ramos, V., 1997. Deep structure of the Metán-Guachipas region: tectonic inversion in north-western Argentina. Journal of South American Earth Sciences 10, 403–421.
de Silva, S., 1989. Altiplano-Puna volcanic complex of the Central Andes. Geology 17, 1102–1106.
de Silva, S., Zandt, G., Trumbull, R., Viramonte, J., Salas, G., Jiménez, M., 2006. Large-scale silicic volcanism in the Central Andes–a tectonomagmatic perspective. In: Troise, C., de Natale, G., Kilburn, C. (Eds.), Mechanisms of Activity and Unrest at Large Calderas, 269. Geological Society of London Special Publication, pp. 47–63.
Echternacht, F., Tauber, S., Eisel, M., Brasse, H., Schwarz, G., Haak, V., 1997. Electromagnetic study of the active continental margin in northern Chile. Physics of the Earth and Planetary Interiors 102, 69–87.
Engdahl, R., van der Hilst, R., Buland, R., 1998. Global teleseismic earthquake relocation with improved travel times and procedures for depth determination. Bulletin of the Seismological Society of America 88, 722–743.
Fromm, R., Zandt, G., Beck, S., 2004. Crustal thickness beneath the Andes and Sierras Pampeanas at 30°S inferred from Pn apparent phase velocities. Geophysical Research Letters 31, doi:10.1029/2003GL019231.
Gangui, A., 1998. A combined structural interpretation based on seismic data and 3-D gravity modelling in the Northern Puna/Eastern Cordillera Oriental, Argentina. Ph. D. Thesis. Freie Universität Berlin, Berlin.
Giambiagi, L., Ramos, V., 2002. Structural evolution of the Andes between 33°30′ and 33°45′ S, above the transition zone between the flat and normal subduction segment, Argentina and Chile. Journal of South American Earth Sciences 15, 99–114.
Giese, P., Scheuber, E., Schilling, F., Schmitz, M., Wigger, P., 1999. Crustal thickening processes in the Central Andes and the different natures of the Moho-discontinuity. Journal of South American Earth Sciences 12, 201–220.
Götze, H.-J., 1984. Über den Einsatz interaktiver Computergraphik im Rahmen 3-dimensionaler Interpretationstechniken in Gravimetrie und Magnetik. Habilitationsschrift. Technische Universität Clausthal, Clausthal.
Götze, H.-J., Kirchner, A., 1997. Interpretation of Gravity and Geoid in the Central Andes between 20° and 29°S. Journal of South American Earth Sciences 10, 179–188.
Götze, H.-J., Lahmeyer, B., Schmidt, S., Strunk, S., Araneda, M., 1990. Central Andes gravity data base. Eos 71, 401–407.
Graeber, F., Asch, G., 1999. Three-dimensional models of P wave velocity and P-to-S velocity ratio in the southern Central Andes by simultaneous inversion of local earthquake data. Journal of Geophysical Research 104, 20237–20256.

Hacker, B., Abers, G., Peacock, S., 2003. Subduction factory 1: theoretical mineralogy, density, seismic wave speeds, and H_2O content. Journal of Geophysical Research 108, doi:10.1029/2001JB001127.

Hacker, B., Abers, G., 2004. Subduction factory 3: an excel worksheet and macro for calculating the densities, seismic wave speeds, and H_2O contents of minerals and rocks at pressure and temperature. Geochemistry Geophysics Geosystems 5, Q01005, doi:10.1029/2003GC000614.

Hamza, V., Muñoz, M., 1996. Heat flow map of South America. Geothermics 25, 599–646.

Hamza, V., Silva Dias, F., Gomes, A., Delgadilho Terceros, Z., 2005. Numerical and functional representations of regional heat flow in South America. Physics of the Earth and Planetary Interiors 152, 223–256.

Heinsohn, W.-D., 1993. Druck und Temperaturabhängigkeit der Geschwindigkeit-Dichte Relation für extrem grosse Krustenmächtigkeiten. Berliner Geowissenschaften Abhandlungen B 20, 131–226.

Heit, B., 2005. Teleseismic tomographic images of the Central Andes at 21°S and 25.5°S: an inside look at the Altiplano and Puna plateaus. Ph. D. Thesis. Freie Universität Berlin, Berlin.

Heit, B., Koulakov, G., Asch, G., Yuan, X., Kind, R., Alcocer-Rodriguez, I., Tawackoli, S., Wilke, H., 2008. More constraints to determine the seismic structure beneath the Central Andes at 21°S using teleseismic tomography analysis. Journal of South American Earth Sciences 25, 22–36.

Henry, S., Pollack, H., 1988. Terrestrial heat flow above the Andean Subduction Zone in Bolivia and Peru. Journal of Geophysical Research 93, 15153–15162.

Hyndman, R., Peacock, S., 2003. Serpentinization of the forearc mantle. Earth and Planetary Science Letters 212, 417–432.

Isacks, B., 1988. Uplift of the Central Andes plateau and bending of the Bolivian Orocline. Journal of Geophysical Research 93, 3211–3231.

Jordan, T., Isacks, B., Allmendinger, R., Brewer, J., Ramos, V., Ando, C., 1983. Andean tectonics related to geometry of the subducted Nazca Plate. Geological Society of America Bulletin 94, 341–361.

Jordan, T., Gardeweg, M., 1989. Tectonic evolution of the late cainozoic Central Andes. In: Ben-Avraham, Z. (Ed.), The Evolution of the Pacific Ocean Margin. Oxford University Press, pp. 193–207.

Kamiya, S., Kobayashi, Y., 2000. Seismological evidence for the existence of serpentinized wedge mantle. Geophysical Research Letters 27 (6), 819–822.

Kay, R., Kay, S., 1993. Delamination and delamination magmatism. Tectonophysics 219, 177–189.

Kay, S., Coira, B., Viramonte, J., 1994. Young mafic back arc volcanic rocks as indicators of continental lithospheric delamination beneath the Argentina Puna plateau, Central Andes. Journal of Geophysical Research 99 (24), 323–324, 339.

Kay, C., Mpodozis, C., Coira, B., 1999. Magmatism, tectonism and mineral deposits of the Central Andes (22–33° S Latitude). In: Skinner, B. (Ed.), Geology and ore deposits of the Central Andes, 7. Society of Economic Geology Special Publication, pp. 27–59.

Kay, S., Coira, B., Caffe, P., 2008. Geoquímica, fuentes y evolución del magmatismo neógeno de la Puna Norte. In: Coira, B., Zappettini, E. (Eds.), Geología y Recursos Naturales de la Provincia de Jujuy. Relatorio 17° Congreso Geológico Argentino, pp. 322–334.

Kirchner, A., Götze, H.-J., Schmidt, S., 1996. 3-D density modelling with seismic constraints in the Central Andes. Physics and Chemistry of the Earth 21 (4), 289–293.

Kley, J., Monaldi, C., Salfity, J., 1999. Along strike segmentation of the Andean foreland: causes and consequences. Tectonophysics 301, 75–94.

Kley, J., Monaldi, C., 2002. Tectonicinversion in the Santa Barbara System of the central Andean foreland thrust belt, north-western Argentina. Tectonics 21, doi:10.1029/2002TC902003.

Lamb, S., 2000. Active deformation in the Bolivian Andes, South America. Journal of Geophysical Research 105, 2627–2653.

Lee, C.-T., Lenardic, A., Cooper, C., Niu, F., Levander, A., 2005. The role of chemical boundary layers in regulating the thickness of continental and oceanic thermal boundary layers. Earth and Planetary Science Letters 230, 379–395.

Lessel, K., 1997. Die Krustenstruktur der zentralen Anden in Nordchile (21–24°S), abgeleitet aus 3D-Modellierungen refraktionsseismischer Daten. Ph.D. Thesis. Freie Universität Berlin, Berlin.

Lucassen, F., Lewerenz, S., Franz, G., Viramonte, J., Mezger, K., 1999. Metamorphism, isotopic ages and composition of lower crustal granulite xenoliths from the Cretaceous Salta Rift, Argentina. Contributions to Mineralogy and Petrology 134, 325–341.

Lucassen, F., Becchio, R., Harmon, R., Kasemann, S., Franz, G., Trumbull, R., Wilke, H.-G., Romer, R., Dulski, P., 2001. Composition and density model of the continental crust in an active continental margin—the Central Andes between 18° and 27°S. Tectonophysics 341, 195–223.

Lucassen, F., Escayola, M., Romer, R., Viramonte, J., Koch, K., Franz, G., 2002. Isotopic composition of Late Mesozoic basic and ultrabasic rocks from the Andes (23–32°S)–implications for the Andean mantle. Contributions to Mineralogy and Petrology 143, 336–349.

McQuarrie, N., DeCelles, P., 2001. Geometry and structural evolution of the central Andean backthrust belt, Bolivia. Tectonics 20, 669–692.

Mooney, W., Laske, G., Masters, T., 1998. Crust 5.1: a global model at 5 degrees × 5 degrees. Journal of Geophysical Research 103, 727–747.

Müller, J., Kley, J., Jacobshagen, V., 2002. Structure and Cenozoic kinematics of the Eastern Cordillera. southern Bolivia (21°S), Tectonics 21, doi:10.1029/2001TC001340.

Müller, R., Roest, W., Royer, J., Gahagan, L., Sclater, J., 1997. Digital lsochrons of the World's Ocean Floor. Journal of Geophysical Research 102B, 3211–3214.

Patzwahl, R., Mechie, J., Schulze, A., Giese, P., 1999. Two-dimensional velocity models of the Nazca plate subduction zone between 19.5°S and 25°S from wide-angle seismic measurements during the CINCA95 project. Journal of Geophysical Research 104, 7293–7317.

Peacock, S.M., 1993. The importante of blueschist–eclogite dehydration reactions in subducting oceanic crust. Geological Society of America Bulletin 105, 684–694.

Pérez-Gussinyé, M., Lowry, A., Phipps Morgan, A., Tassara, A., 2008. Effective elastic thickness variations along the Andean margin and their relationship to subduction geometry. Geochemistry, Geophysics, Geosystems 9 (2), doi:10.1029/2007GC001786.

Pérez-Gussinyé, M., Swain, C., Kirby, J., Lowry, A., 2009. Spatial variations of the effective elastic thickness, Te, using multitaper spectral estimation and wavelet methods: examples from synthetic data and application to South America. Geochemistry, Geophysics, Geosystems 10 (4), doi:10.1029/2008GC002229.

Ramos, V., Cristallini, E., Pérez, D., 2002. The Pampean flat-slab of the Central Andes. Journal of South American Earth Sciences 15, 59–78.

Rudnick, R., Fountain, D., 1995. Nature and composition of the continental crust: a lower crustal perspective. Reviews of Geophysics 33, 267–309.

Scheuber, E., Bogdanic, T., Jensen, A., Reutter, K., 1994. Tectonic development of the north Chilean Andes in relation to plate convergence and magmatism since the Jurassic. In: Reutter, K., Scheuber, E., Wigger, P. (Eds.), Tectonics of the southern Central Andes, Berlin Heidelberg New York, pp. 7–22.

Schilling, F., Partzsch, G., 2001. Quantifying partial melt fraction in the crust beneath the Central Andes and the Tibetan plateau. Physics and Chemistry of the Earth (A) 26, 239–246.

Schilling, F., Partzsch, G., Brasse, H., Schwarz, G., 1997. Partial melting below the magmatic arc in the Central Andes deduced from geoelectromagnetic field experiments and laboratory data. Physics of the Earth and Planetary Interiors 103, 17–32.

Schilling, F., Trumbull, R., Brasse, H., Haberland, C., Asch, G., Bruhn, D., Mai, K., Haak, V., Giese, P., Muñoz, M., Ramelow, J., Rietbrock, A., Ricaldi, E., Vietor, T., 2006. Partial melting in the Central Andean crust: a review of geophysical, petrophysical, and petrologic evidence. In: Oncken, O., Chong, G., Franz, P., Giese, P., Götze, H.-J., Ramos, V., Strecker, M., Wigger, P. (Eds.), Frontiers in Earth Sciences. Vol. 1. The Andes–Active Subduction Orogeny. Springer Verlag, Berlin, Heidelberg, pp. 459–474.

Schmidt, S., Götze, H.-J., 1999. Integration of data constraints and potential field modelling—an example from southern Lower Saxony, Germany. Physics and Chemistry of the Earth (A) 24, 191–196.

Schmitz, M., Kley, J., 1997. The geometry of the Central Andean back arc crust: joint interpretation of cross-section balancing and seismic refraction data. Journal of South American Earth Sciences 10, 99–110.

Schmitz, M., Heinsohn, W., Schilling, F., 1997. Seismic, gravity and petrological indications for partial melting beneath the thickened Central Andean crust 21°–23°S. Tectonophysics 270, 313–326.

Schmitz, M., Lessel, K., Giese, P., Wigger, P., Araneda, M., Bribach, J., Graeber, F., Grunewald, S., Haberland, C., Lüth, S., Röwer, P., Ryberg, T., Schulze, A., 1999. The crustal structure beneath the Central Andean fore arc and magmatic arc as derived from seismic studies—the PISCO 94 experiment in northern Chile (21–23°S). Journal of South American Earth Sciences 12, 237–260.

Schurr, B., Asch, G., Rietbrock, A., Trumbull, R., Haberland, C., 2003. Complex patterns of fluid and melt transport in the central Andean subduction zone revealed by attenuation tomography. Earth and Planetary Science Letters 215, 105–119.

Schurr, B., Rietbrock, A., 2004. Deep seismic structure of the Atacama basin. northern Chile, Geophysical Research Letters 31, doi:10.1029/2004GL019796.

Schwarz, G., Krüger, D., 1997. Resistivity cross section through the southern Central Andes as inferred from magnetotelluric and geomagnetic deep soundings. Journal of Geophysical Research 102, 11957–11978.

Sick, C., Yoon, M., Rauch, K., Buske, S., Lüth, S., Araneda, M., Bataille, K., Chong, G., Giese, P., Krawczyk, Ch., Mechie, J., Meyer, H., Oncken, O., Reichert, C., Schmitz, M., Shapiro, S., Stiller, M., Wigger, P., 2006. Seismic images of accretive and erosive subduction zones from the Chilean Margin. In: Oncken, O., Chong, G., Franz, P., Giese, P., Götze, H.-J., Ramos, V., Strecker, M., Wigger, P. (Eds.), Frontiers in Earth Sciences. Vol. 1. The Andes–Active Subduction Orogeny. Springer Verlag, Berlin, Heidelberg, pp. 147–169.

Sobolev, S., Babeyko, A., 1994. Modelling of mineralogical composition, density and elastic wave velocities in anhydrous magmatic rocks. Surveys in Geophysics 15, 515–544.

Springer, M., Förster, A., 1998. Heat-flow density across the Central Andean subduction zone. Tectonophysics 291, 123–139.

Springer, M., 1999. Interpretation of heat-flow density in the Central Andes. Tectonophysics 306, 377–395.

Stern, C., 2004. Active Andean volcanism: its geologic and tectonic setting. Revista Geológica de Chile 31, 161–206.

Stern, R., 2002. Subduction zones. Reviews of Geophysics 40, doi:10.1029/2001RG000108.

Tassara, A., 2006. Factors controlling the crustal density structure underneath active continental margins with implications for their evolution. Geochemistry Geophysics Geosystems 7, doi:10.1029/2005GC001040.

Tassara, A., Götze, H.-J., Schmidt, S., Hackney, R., 2006. Three-dimensional density model of the Nazca plate and the Andean continental margin. Journal of Geophysical Research 111, doi:10.1029/2005JB003976.

Tassara, A., Swain, C., Hackney, R., Kirby, J., 2007. Elastic thickness structure of South America estimated using wavelets and satellite-derived gravity data. Earth and Planetary Science Letters 253, 17–36.

Turcotte, D., Schubert, G., 2002. Geodynamics. Cambridge University Press, New York, pp. 456.

Wigger, P., Schmitz, M., Araneda, M., Asch, G., Baldzuhn, S., Giese, P., Heinsohn, W.-D., Martínez, E., Ricaldi, E., Röwer, P., Viramonte, J., 1994. Variation in the Crustal Structure of the Southern Central Andes Deduced from Seismic Refraction Investigation. In: Reutter, K., Scheuber, E., Wigger, P. (Eds.), Tectonics of the southern Central Andes. Springer, Berlin Heidelberg New York, pp. 23–48.

Withman, D., Isacks, B., Kay, S., 1996. Lithospheric structure and along-strike segmentation of the Central Andean Plateau: seismic Q, magmatism, flexure, topography and tectonics. Tectonophysics 259, 29–40.

Wörner, G., Lezaun, J., Beck, A., Heber, V., Lucassen, F., Zinngrebe, E., Rösling, R., Wilke, H.-G., 2000. Geochronology, metamorphic petrology and geochemistry of basement rocks from Belén (N. Chile) and C. Uyarani (W. Bolivian Altiplano): implications for the evolution of Andean basement. Journal of South American Earth Sciences 13, 717–737.

Yoon, M., Buske, S., Lüth, S., Schulze, A., Shapiro, S., Stiller, M., Wigger, P., 2003. Along-strike variations of crustal reflectivity related to the Andean subduction process. Journal of Geophysical Research 30, doi:10.1029/2002GL015848.

Yuan, X., Sobolev, S., Kind, R., Oncken, O., Andes Working Group, 2000. Subduction and collision processes in the Central Andes constrained by converted seismic phases. Nature 408, 958–961.

Yuan, X., Sobolev, S., Kind, R., 2002. Moho topography in the Central Andes and its geodynamic implications. Earth and Planetary Sciences Letters 199, 389–402.

Zandt, G., Leidig, M., Chmielowski, J., Baumont, D., Yuan, X., 2003. Seismic detection and characterization of the Altiplano-Puna magma body, Central Andes. Pure and Applied Geophysics 160, 789–807.